REVIEW

Check for updates

Recent advances in conjugated microporous polymers for photocatalysis: designs, applications, and prospects

Songhao Luo,†[a] Zhuotong Zeng,†[b] Guangming Zeng, [ID] *[a] Zhifeng Liu, [ID] *[a] Rong Xiao,*[b] Piao Xu,[a] Han Wang, [ID][a] Danlian Huang, [ID][a] Yang Liu,[a] Binbin Shao,[a] Qinghua Liang,[a] Dongbo Wang,[a] Qingyun He,[a] Lei Qin[a] and Yukui Fu[a]

Solar energy is a clean and sustainable energy source. Natural photosynthesis has existed for millions of years, which can convert solar energy into chemical energy needed by living things. Inspired by natural photosynthesis, scientists have developed a series of artificial photosynthetic systems that can use solar energy efficiently for humans. Conjugated microporous polymers (CMPs) are a new class of materials that can be used in artificial photosynthetic systems. This review illustrates the light–harvesting capability and the energy transfer phenomena within the supramolecular structure of CMPs to provide guidelines for the rational design of these polymers with excellent photocatalytic properties and systematically discusses the applications of these materials in the field of photocatalysis including photocatalytic water splitting, CO_2 reduction, organic conversion, environmental remediation, and medical health. Finally, this review points out the major challenges in this topic and suggests the next feasible development direction.

1. Introduction

Since the industrial revolution, the average living standard of human beings has increased, and the demand for energy has also grown rapidly. Energy is one of the key factors determining social and economic development, especially in developing countries. At present, the main energy used in the world is fossil energy.[1–3] It has two main shortcomings: (i) its limited earth storage cannot support the long-term high-speed development of human beings; (ii) the massive use of fossil energy has a negative impact on the environment. Therefore, it is necessary to explore new energy sources to provide new directions for global development. Solar energy is widely considered to be a low-cost, clean and abundant source of energy.[4–6] The solar energy received on Earth is much higher than the human demand for energy. The use of solar energy is undoubtedly an effective strategy to improve the energy structure and improve the global ecological environment. The question now is how to

[a]*College of Environmental Science and Engineering, Hunan University and Key Laboratory of Environmental Biology and Pollution Control (Hunan University), Ministry of Education, Changsha 410082, P. R. China. E-mail: zgming@hnu.edu.cn; zhifengliu@hnu.edu.cn*

[b]*Department of Dermatology, Second Xiangya Hospital, Central South University, Changsha 410011, P. R. China. E-mail: xiaorong65@csu.edu.cn*

† These authors contributed equally to this work.
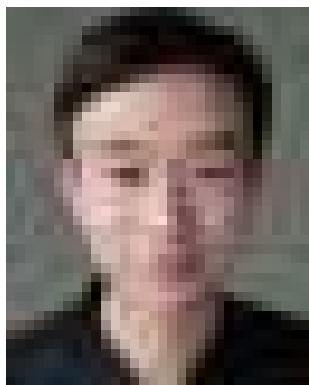
Songhao Luo is a Ph.D. candidate under the supervision of prof. Guangming Zeng at the College of Environmental Science and Engineering, Hunan University, China. His current research interests focus on preparing functional porous materials applied in various fields such as energy storage and photocatalysis.
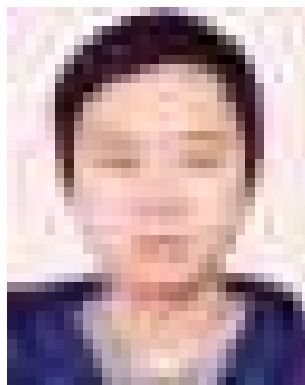
M.D. Zhuotong Zeng obtained his M.B. in July 2009, M.M. in July 2012, and M.D. in December 2019 from the Xiangya Medical College of Central South University. He now is working as an assistant professor in Xiao's group at the Second Xiangya Hospital. His current research interests focus on the application of advanced functional nanomaterials for environmental medicine.

6434 | *J. Mater. Chem. A*, 2020, **8**, 6434–6470

This journal is © The Royal Society of Chemistry 2020

efficiently convert solar energy into a chemical energy source for human use.

Photosynthesis, also known as photo-energy synthesis, refers to converting solar energy into chemical energy by photosynthetic pigments or some natural photocatalysts in photosynthetic organisms under visible light irradiation. This unique biochemical process has existed in nature for millions of years. Inspired by natural photosynthesis, researchers have innovatively developed a range of artificial systems and devices that use organic and/or inorganic materials to simulate natural photosynthesis.[7–13] They provide an effective way to convert solar energy into chemical energy.

The first successful attempt to convert solar energy into chemical energy was made in 1972 when Fujishima and Honda found that TiO_2 electrodes could promote photocatalytic water decomposition.[14] As early as 2008, Fujishima reviewed the origin of TiO_2 photocatalysts based on the information available at that time and pointed out the potential development direction.[15] With the development of photocatalysis technologies, other materials have also attracted the attention of scientists. For example, mature transition metal complexes have been developed in recent years.[16–22] In addition, there are other hot metal-free and semiconductor materials,[23,24] such as graphene,[25] reduced graphene oxide,[26–28] g-C_3N_4,[29–33] and polyoxometalates (POMs).[34–36] However, these materials have some disadvantages which are difficult to overcome: (i) they are unstable and short in service life; (ii) most noble metal materials are expensive and have low reserves in nature; (iii) these catalysts are extremely toxic to the ecological environment; (iv) they will be corroded by the reaction solvent in the reaction medium, thereby affecting the performance of the catalyst after recovery. Therefore, it is necessary to develop more types of heterogeneous photocatalysts with high stability and reusability.[37–40]

Recently, scientists have extensively studied the existing nanoporous heterogeneous catalytic materials.[41,42] The nanometer properties help to achieve a higher specific surface area,[43,44] and the porous properties help to provide additional catalytically active sites.[45–47] Plasmon metal nanomaterials have surface plasmon resonance (SPR) properties, which give them an unique ability to collect electromagnetic fields and convert photon energy into heat energy, showing great application potential in the field of photocatalysis.[48] Owing to their regularity and synthesis of adjustable structures, metal organic frameworks (MOFs) can contain a photosensitizer and catalytic center in a single structure and provide a channel structure to promote the spread of the substrate and product. As a light-harvesting antenna and catalytic center, they have been proved to be quite effective in light capture, photocatalytic proton reduction, CO_2 reduction, and photocatalytic degradation of organic pollutants.[49,50] Meanwhile, adjustable covalent organic frameworks (COFs) can be used to obtain photocatalytic systems with excellent photocatalytic performance.[51] (i) Modularity: COFs are composed of molecular building blocks, and the basic functions of their photocatalytic process can be regulated by adjusting the molecular structure. (ii) Porosity: the high porosity of COFs provides a high specific surface area, which allows charge to spread rapidly on the surface. (iii) Crystallinity: the periodic structural units of COFs facilitate the transfer of charge and prevent the recombination of charge
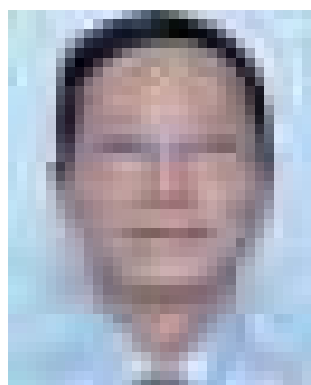

Prof. Guangming Zeng has been teaching courses and performing research on Environmental Science and Health at Hunan University since 1988. He has been heading the School of Environmental Science and Engineering since 1994 at the same University. He is one of the 2017 and 2018 Highly Cited Researchers in the world issued by Clarivate Analytics. His group has worked on a variety of research areas, including nanotechnology for energy storage, cleaner production, ecological remediation, and environmental medicine.
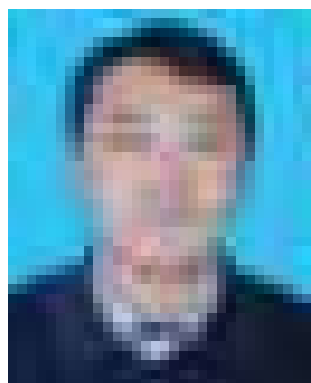
Dr Zhifeng Liu is now an associate professor at Hunan University. He has published more than 80 peer-reviewed papers with more than 2600 citations. He has applied for more than 30 national invention patents (19 authorized), more than 20 national utility model patents (14 authorized), and 2 international invention patents. He is mainly engaged in the application of functional nanomaterials in environmental remediation.
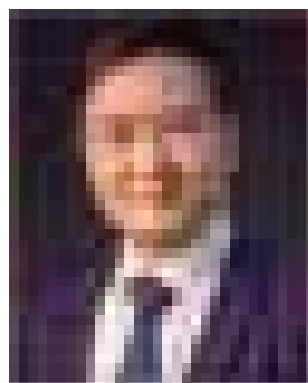
Prof. Rong Xiao has been engaged in clinical work since 1987 at the Second Xiangya Hospital which is the best hospital in Hunan province with 60 million people. In 2008, he was named the China outstanding young dermatologist. His honors include the 2017 National Science and Technology Progress Award of China (the second Award, ranked third). His current research interests including nanotechnology for environmental medicine.

This journal is © The Royal Society of Chemistry 2020

J. Mater. Chem. A, 2020, **8**, 6434–6470 | **6435**

carriers. (iv) COFs are composed of lightweight elements through covalent bonds, so they have stability, low density, and high gravimetric performance. These properties indicate the potential of COFs in photocatalytic technology research.

Among various nanoporous materials, conjugated microporous polymers (CMPs) are emerging material platforms. CMPs have a π-conjugated backbone and a permanent porous structure that distinguish them from unstable porous materials and non-porous conjugated polymers, which were first synthesized by Cooper's group in 2007.[52] Since their first synthesis, they have been widely studied as an attractive platform for catalytic, energy storage, environmental remediation *etc.*, which can be proved by the number of "Conjugated microporous polymer" keyword indexed journals that have increased year by year over the past decade (Fig. 1). There are now more than 200 research groups around the world studying CMPs which are on the rise. In 2013, Jiang's group reviewed the design principles, synthesis, and structure of CMPs, and discussed the application of CMPs.[53] They present the properties of CMP materials which are easily regulated by synthesis control such as (i) adjustment of the length and geometric structure of monomers, (ii) use of statistical copolymerization strategies, and (iii) adjustment of reaction conditions.

Compared to traditional inorganic semiconductor materials, CMPs have unique advantages such as low cost, permanent nanopores, high porosity, and high activity and stability, as well as adjustable photoelectric properties, and have recently been extensively researched as photocatalysts.[54–58] Few reviews comprehensively and in detail discuss the latest progress of CMPs in the field of photocatalysis, and it is time to fully review the advancements of CMPs in the field of photocatalysis to promote the further development of CMP materials and photocatalysis technology. Therefore, in this review, we aim to summarize recent progress in using CMPs as a robust platform for artificial photosynthesis and photocatalysis. Firstly, the review introduces the light-harvesting and energy transfer phenomena of CMP materials and provides guidelines for the rational design of CMPs with excellent photocatalytic

Fig. 1 Evolution of the number of publications concerning the keywords "Conjugated microporous polymer" in indexed journals between 2009 and 2019. The data come from the research on "web of science".

performances. Secondly, it extends the photocatalytic applications (*e.g.* photocatalytic water splitting and CO_2 conversion, organic conversion, and wastewater treatment). Finally, the review presents existing limitations in the field and proposes future research prospects. CMP materials have brought about new vitality to the field of photocatalysis, and further basic research and application exploration are needed. We hope this review will inspire the interest of readers in the fields of materials science, engineering technology, energy science, and environmental science.

2.   Basic concept and improvement strategy of CMPs for photocatalysis

2.1   Basics of constructing efficient CMP photocatalysts

In nature, the most common photosynthetic unit is a complex network of chlorophyll proteins. According to the structure classification (Fig. 2),[59] they can be divided into spherical,[60,61] lamellar,[62,63] and tubular.[64,65] In these molecular or supramolecular structures, the absorbed photons produce an excited state on the photosensitive pigment molecules upon receipt of solar energy. This excited state is transported between the phytochrome molecules and eventually transferred to the photoreaction center. In the photoreaction center, the excitation energy is used for charge separation, and active excitation energy is converted into stable chemical energy.

Inspired by natural photosynthesis, scientists have established a variety of artificial photosynthetic systems. CMPs are one of the finest platforms for these systems that combine an adjustable conjugated skeleton with a permanent microporous structure. Their skeleton acts as a funnel, and the captured energy of the skeleton quickly transfers to the encapsulated guest material. As shown in Fig. 3a, polyphenylene-based CMPs (PP-CMPs) emit blue photoluminescence, which excites energy to migrate across the framework and the charge can be transferred rapidly (0.04 cm^2 V^{-1} s^{-1}).[66] The micropores of PP-CMPs encapsulate the energy acceptor coumarin 6. The excitation energy on the PP-CMP backbone will be rapidly directed to the coumarin 6 molecule under the synergy of an average of 176 phenylene units. The fast, efficient and vector efficiency of energy transfer efficiency of PP-CMPs is because of the unique structure. The structure constitutes a spatial confinement for coumarin 6 molecules to make the light-harvesting systems with high efficiency possible. As another example, two fluorescent pyrene-based CMPs (**Py-PP** and **Py-BPP**) rendered with the pyrene chromophore also have excellent light-harvesting properties because the excitation energy of the mainframe is quickly and efficiently transferred to the encapsulated guest molecules (Fig. 3b).[67] These unique characteristics clearly originate from their conjugated porous structure and demonstrate the usefulness of CMPs in the investigation of a simulated natural light-harvesting supramolecular structure.

The design of artificial photosynthetic systems requires not only light harvesting in a limited nanospace but also the interaction of the various units to achieve efficient energy transfer. CMP materials that are constructed from electron
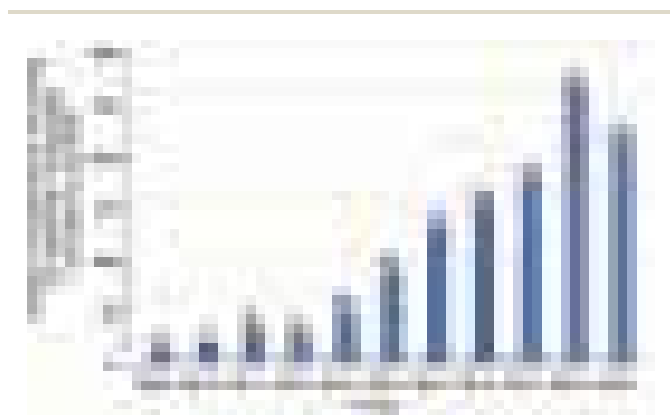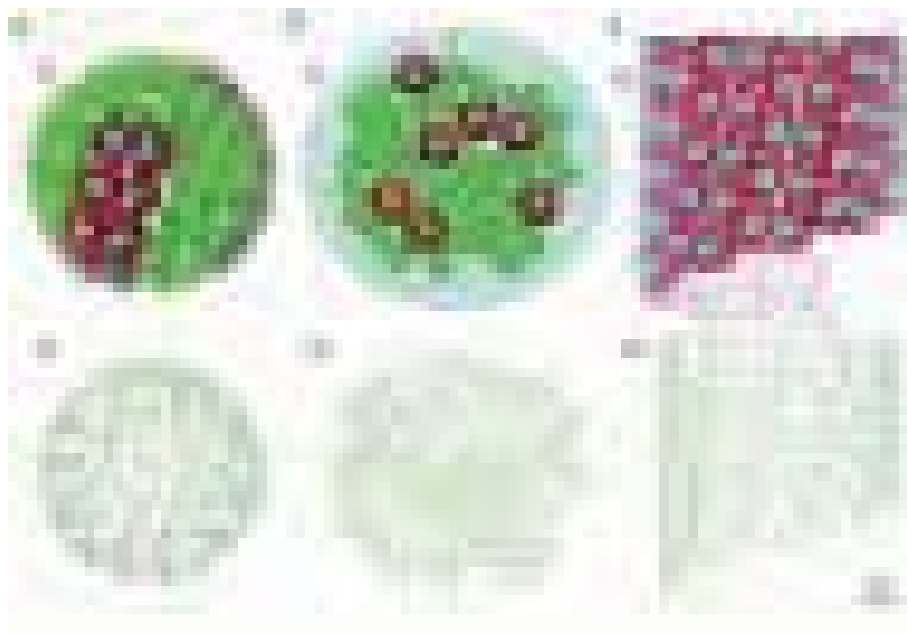
Fig. 2 Schematic structural model of the common photosynthetic unit. (a) Spherical, (b) lamellar, and (c) tubular. Light-harvesting complex 2 (LH2) in green; reaction center-light-harvesting complex 1 (RC–LH1) (LH1 in red; RC in blue). Reprinted with permission from ref. 59. Copyright 2011 Wiley-VCH Verlag GmbH & Co. KGaA, Weinheim.

donor or electron acceptor units can be transformed to achieve the blending of highest occupied molecular orbital (HOMO) and lowest unoccupied molecular orbital (LUMO) energy levels, which can effectively improve energy conversion efficiency.[68–70] As shown in Fig. 4a and b, in a ternary system, benzo[1′,2′-*c*:4′,5′-*c′*]dithiophene-4,8-dione))]; 3,9-bis(2-methylene-(3-(1,1-dicyanomethylene)-indanone))-5,5,11,11-tetrakis(4- hexylphenyl)-dithieno[2,3-*d*:2′,3′-*d′*]-*s*-indaceno[1,2-*b*:5,6-*b′*] dithiophene (ITIC) acts as an acceptor, and the benzodithiophene-*alt*-fluorobenzotriazole copolymer (J51) and poly[[2,6-(4,8-bis(5-(2-ethylhexyl)thiophen-2-yl)-benzo[1,2-*b*:4,5-*b′*]dithiophene))-*alt*-(5,5-(1′,3′-di-2-thienyl-5′,7′-bis(2-ethylhexyl) (PBDB-T) are incorporated as donors.[71] This ternary system has good light-harvesting ability and charge transport capability owing to

Fig. 3 (a) Schematic representation of energy funneling from PP-CMP to spatially confined coumarin 6. Reprinted with permission from ref. 66. Copyright 2010 American Chemical Society. (b) Schematic representation of the light-harvesting process from a porous polymer framework to entrapped chromophores. Reprinted with permission from ref. 67. Copyright the Owner Societies 2016.
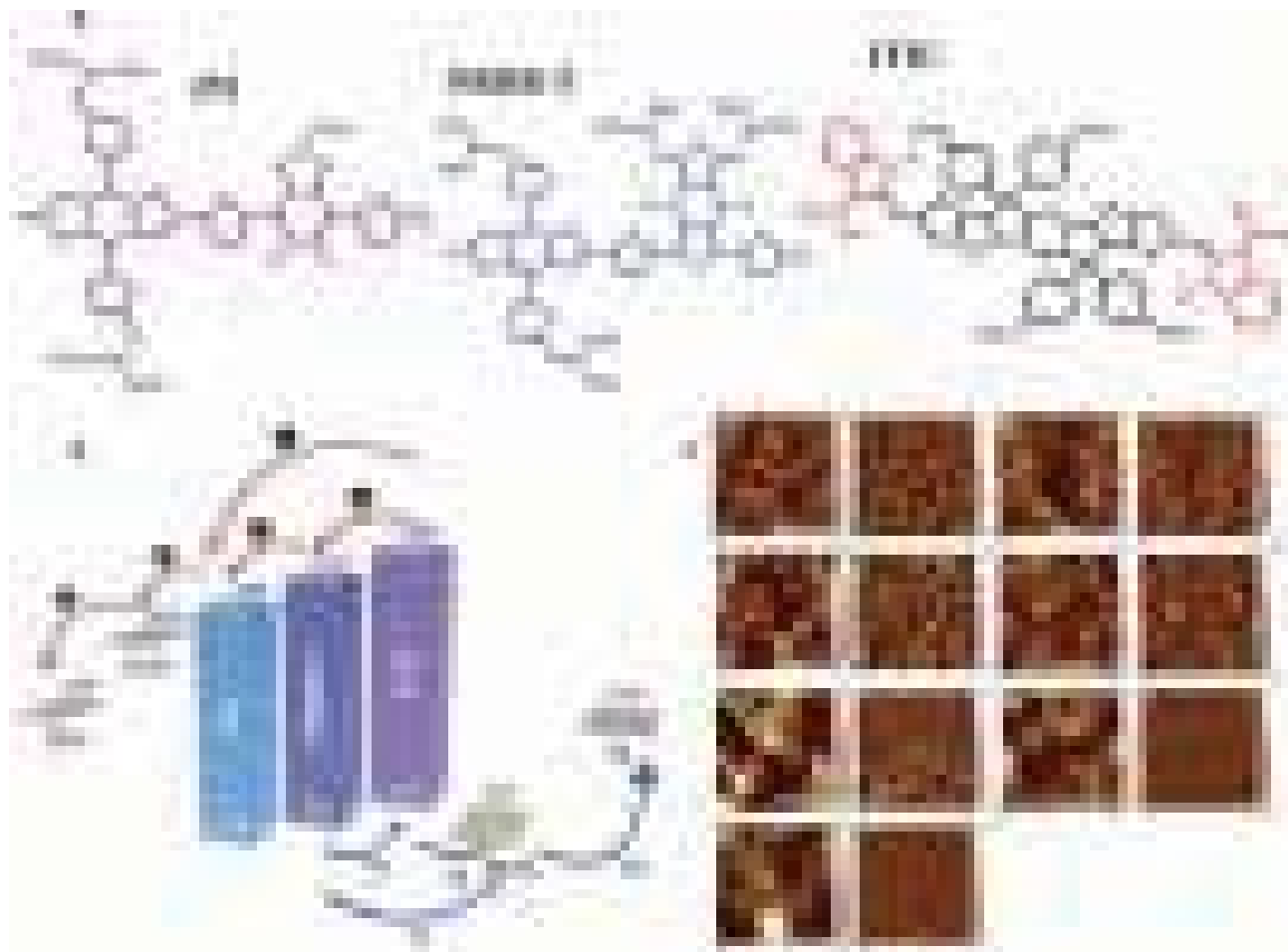
This journal is © The Royal Society of Chemistry 2020

J. Mater. Chem. A, 2020, **8**, 6434–6470 | **6437**

Fig. 4 (a) Chemical structures of benzodithiophene-*alt*-fluorobenzotriazole copolymer J51, PBDB-T, and ITIC. (b) Appropriate energy level matching of the ternary system. (c) Tapping-mode AFM (1 × 1 μm) images (left: topographic images and right: phase images) of blend films deposited with different ratios of J51/PBDB-T/ITIC. Reprinted with permission from ref. 71. Copyright 2018 American Chemical Society.

the light capture capabilities of each material and complementary and tandem energy levels between the materials. Fig. 4c confirms that: (i) different monomer doping ratios affect optical characteristics, (ii) an appropriate doping ratio helps to reduce joint defects, and (iii) adding an appropriate amount of crystal phase improves effectively the surface properties of the thin film in the planar binary system. This strategy suggests that in order to build a type of highly efficient artificial photosynthesis system, in addition to considering the charge separation and migration efficiency of a single CMP surface, we also can design and synthesize binary or multiple CMP systems to achieve efficient solar energy conversion.

2.2 Strategies to improve the photocatalytic performances of CMPs

As early as the late 1990s and early 2000s, many scientists discovered that conjugated polymers have luminescence and semiconducting properties.[72–75] These polymers can be formed by extending the π-conjugated system.[52,76–81] As an example, CMP materials were first reported in 2007.[52] Then various CMPs have emerged such as thiophene-containing CMPs,[82] light-emitting CMPs,[83] soluble CMPs,[84] core–shell CMPs,[85] CMP films,[86] comonomer doped CMPs,[87] tetraphenylethylene-interweaving CMPs,[88] and so on (Fig. 5). The photocatalytic performances of these polymers are highly dependent on their surface area, linkage geometry, conjugation degree, and band gap.[89,90] In recent years, in order to improve the photocatalytic performances of CMP materials, scientists have proposed various improvement strategies.

The molecular structure of CMPs can be regulated by adjusting synthesis methods, reaction conditions, and monomer types, which has been proven to be one of the main strategies to improve their photocatalytic performances. As long ago as 2008, Cooper's group made continuous fine-tuning of CMPs by changing the length of the monomer for the first time, confirming that the statistical copolymerization method can systematically control the chemical structure and bandgap of CMPs.[77] This provides a useful strategy for the direct synthesis control of the microporous nature of CMP photocatalysts. In 2016, a series of benzothiazole CMPs having highly photocatalytic efficiency with 2320 μmol h^{-1} g^{-1} for H$_2$ evolution reactions (HERs) from water splitting were reported.[91] The

Fig. 5   Selected representative existing CMPs with a different time period. (a) CMPs were first synthesized. Reprinted with permission from ref. 52. Copyright 2007 Wiley-VCH. (b) Thienyl-containing CMPs. Reprinted with permission from ref. 82. Copyright 2009 Wiley-VCH. (c) Light-Emitting CMPs. Reprinted with permission from ref. 83. Copyright 2011 American Chemical Society. (d) Soluble CMPs. Reprinted with permission from ref. 84. Copyright 2012 Wiley-VCH. (e) Core−shell CMPs. Reprinted with permission from ref. 85. Copyright the Royal Society of Chemistry 2013. (f) CMP films. Reprinted with permission from ref. 86. Copyright 2014 Wiley-VCH. (g) Comonomer doped CMPs. Reprinted with permission from ref. 87. Copyright 2016 American Chemical Society. (h) Tetraphenylethylene-interweaving CMPs. Reprinted with permission from ref. 88. Copyright 2018 Wiley-VCH.

results show that the introduction of 3D properties into these linear polymer networks will vastly reduce the photocatalytic efficiency. The higher photocatalytic efficiency of linear polymers than their three-dimensional (3D) crosslinked polymer counterparts may be attributed to their high efficiency of charge transfer, separation, and electron transfer.

The surface area and porous structure of CMP materials can be adjusted easily by using SiO_2 nanoparticles (NPs) as a template.[92] In this method, a strong electron-withdrawing group is bonded to a weak electron-donating group through a plurality of C_{sp}–C_{sp} bonds to form a fully conjugated network with specific electronic properties and porous structures. The Brunauer–Emmett–Teller (BET) surface area of the formed CMPs is double that of a polymer network synthesized without using SiO_2 NPs as a template. Furthermore, their photocatalytic performances and long-term stability of photocatalysis[93] can be improved by changing the monomer distribution and/or introducing comonomers with a specific quality. In 2011, a series of CMPs based on pyrene units have been synthesized by statistical copolymerization.[94] These conjugated polymerization networks all have fixed micropores and a high degree of photoluminescence. The photoelectrical properties of pyrene-based CMPs can be fine-tuned by the introduction of luminescent chromophores and by adjusting the distribution of monomers.

Introducing strong electron donors and weak electron acceptors into CMP molecular networks and adjusting the ratio of donor to acceptor can effectively enhance the photocatalytic activity of CMPs.[95] A series of donor–π–acceptor (D–π–A) CMPs with different polymer structures and components were synthesized by using hydrazine, benzothiadiazole, and biphenyl as electron acceptors, electron donors or π-crosslinkers, respectively (Fig. 6).[96] These polymer networks with a D–π–A

structure can expand the light absorption range and can effectively separate photo-generated charges, thereby enhancing the photocatalytic performances of these materials.[97,98] These findings demonstrate the modular nature of CMP materials, and reveal that the profound structural effects provide a basic idea for the rational design of CMP photocatalysts. Considering various electron donors and electron acceptor units, selecting appropriate electron donor and electron acceptor units will build enough D–π–A CMP photocatalysts with enhanced photocatalytic properties, which display a bright future for photocatalytic applications.

In addition to the molecular structure, the morphology will also affect the photocatalytic performances of CMP materials. CMPs are often synthesized as insoluble and unmachinability powders,[99,100] which are not conducive to popularization. To solve this problem, scientists tried to change the shape of CMPs, and a quintessential example is CMP films. They can be synthesized by an electropolymerization method. In this method, the precursor material undergoes a coupling reaction at the surface of the electrode, and a polymer film is deposited on the surface of the electrode. The thickness of the films is controllable during the synthesis and ranges from nanometers to micrometers. However, previous electropolymerization methods were only studied for N-substituted carbazole units.[86,101] The synthesized porous organic polymer films do not have a π-conjugated structure. In 2015, Jiang's group reported for the first time the controllable synthesis of a π-CMP film (thiophene-based CMP film).[102] The porosity, bandgap, conductivity, and prominence of these materials in solar energy conversion systems were explored in this paper. The key to constructing a thiophene-based CMP film is shown in Fig. 7a (blue arrows), that is each thienyl subunit has only one reaction
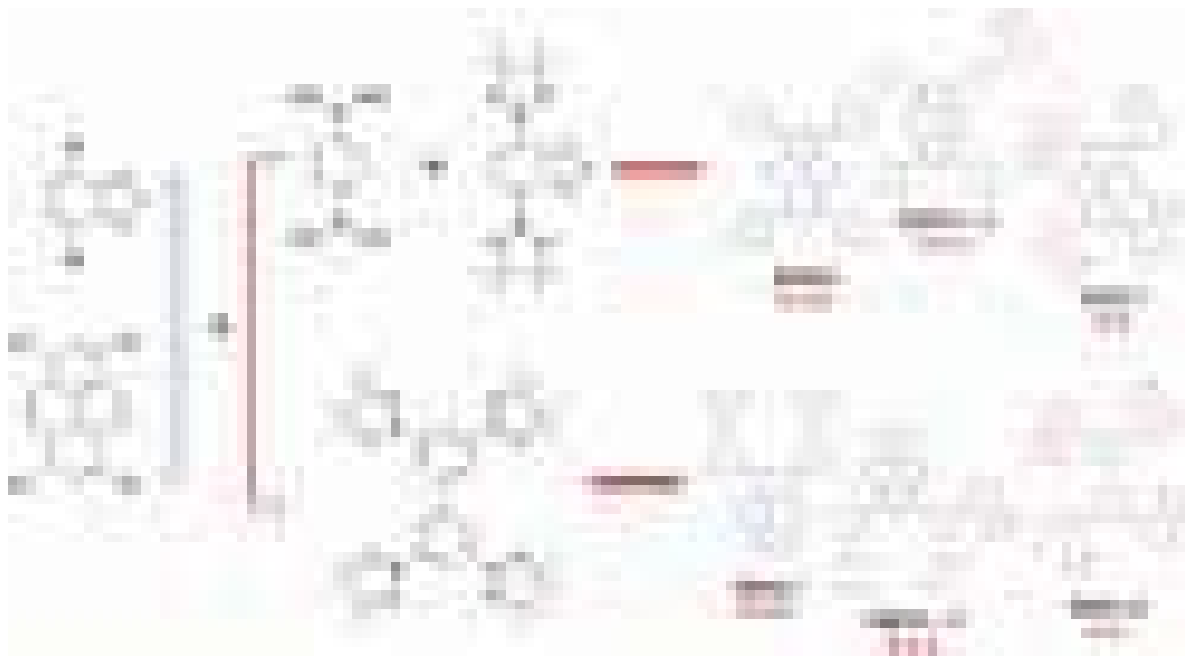
Fig. 6 Synthetic routes to polymers and notional polymer structures. Reprinted with permission from ref. 96. Copyright 2018 Elsevier B.V. All rights reserved.

site. Thienyl groups are connected by C–C bonds to form a π-conjugate structure under the action of electropolymerization (Fig. 7b). Fig. 7c shows the predicted by computational simulation optimized basic single-hole structure (the inset shows a photo of the films). In these CMP films, benzotrithiophene (BTT) and 1,3,5-tri(2-thienyl)-benzene (TTB) play a major role in controlling the growth direction, conductivity, and photoelectric properties of these porous networks. As shown in Fig. 7d, the BTT-CMP films exhibited HOMO and LUMO levels of −5.32 and −3.32 eV, respectively, the TTB-CMP films exhibited HOMO and LUMO levels of −0.54 and −3.19 eV, respectively, and C_{60} matched the energy levels of these polymer films and can be selected as electron acceptors. Therefore, C_{60} was doped into the CMP networks to accelerate charge carrier separation to enhance photoelectric properties (Fig. 7e). This strategy can be extended further to other monomer molecules, which provides guidance for exploring π-CMP films with higher photocatalytic properties.

Stable CMP networks provide excellent support and protection for other active photocatalytic components, which is conducive to forming composite photocatalysts with high photocatalytic activity and stability. Many reported photocatalytic CMPs fall into the "naked" photocatalyst category. Namely, these CMP photocatalysts are constructed by conjugated bonding using various bridging ligands having photocatalytic activity without other additional components. In order to facilitate the catalysis of valuable but intricate and formidable reactions, multiple functional components can be introduced into CMP networks through advanced design to form synergistic photocatalysts. The introduction of different functional nanomaterials (*e.g.* transition metal elements,[103–105] other semiconductor materials,[106,107] and so on) into CMPs can produce a synergistic interaction between the components to provide enhanced photocatalytic performances.

3. CMPs for photocatalytic water splitting

3.1 CMPs for photocatalytic H$_2$ evolution reactions

The conversion of solar energy into clean chemical energy in artificial photosynthetic systems is a well-received project to promoted clean energy instead of fossil energy, which is beneficial to solving global energy and environmental problems. Photocatalytic water splitting is a promising solution among these technologies, which can convert solar energy into valuable hydrogen energy.[108–114] Hydrogen energy is a green, sustainable energy source with three times the gravimetric energy density of gasoline.[114–117] However, the photocatalytic hydrogen production strategy still faces many challenges all around the world.[118–121] Therefore, it is still necessary to explore more types of materials with the required properties for artificial photosynthetic systems. In general, the materials used in photocatalytic hydrogen production from water need to meet the following conditions: (i) stability against the corrosion of water; (ii) a suitable band edge position to meet water redox potential; (iii) a suitable band gap to capture more visible photons to generate enough carriers to facilitate the reduction of protons; (iv) suitable energy band structures to facilitate the migration of charge carriers in polymer units; (v) suitable surface chemical reactions. CMP materials are novel heterogeneous photocatalysts composed of a π-conjugated system with potential for meeting these requirements and have gained many research advances in recent years.[122–125]

6440 | *J. Mater. Chem. A*, 2020, **8**, 6434–6470

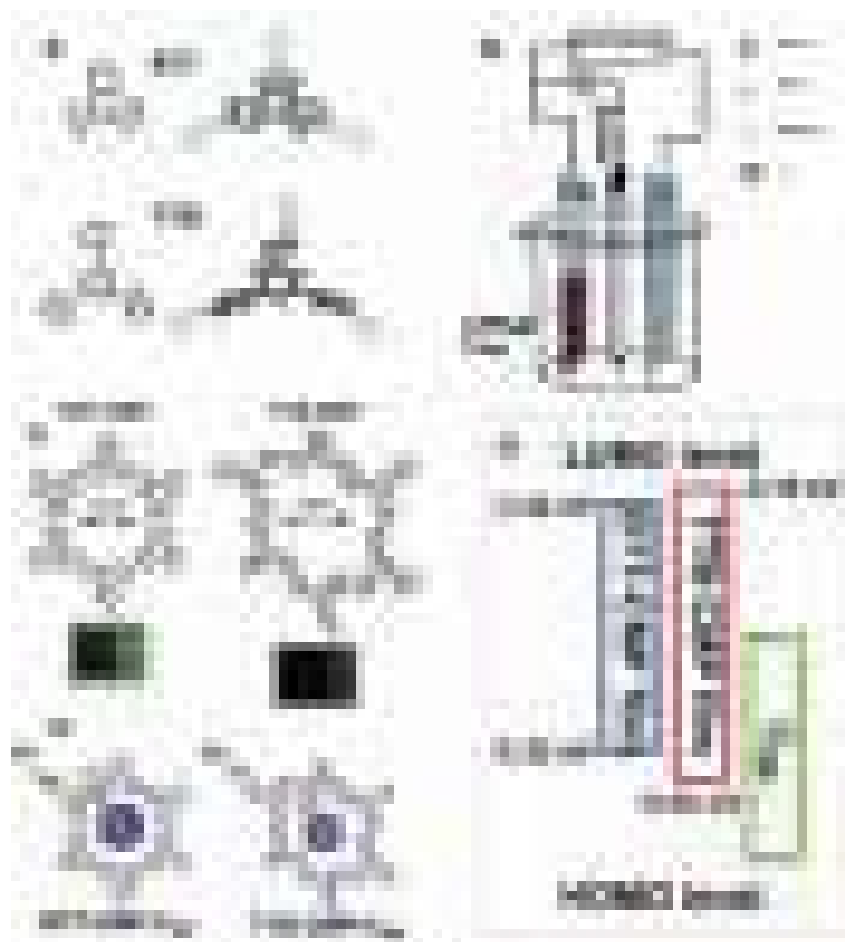This journal is © The Royal Society of Chemistry 2020

Fig. 7 (a) Structure of thiophene-based monomers BTT and TTB; (b) device of the three-electrode cell for the polymerization of monomers and the formation of CMP films on indium tin oxide (ITO). (c) Basic pore structures of the BTT-CMP and TTB-CMP films (inset: photos of the films). (d) HOMO−LUMO levels of the BTT-CMP and TBB-CMP films compared with that of C_{60}; (e) the basic structure of the CMP skeletons and C_{60}. Reprinted with permission from ref. 102. Copyright 2015 The Authors. Published by Wiley-VCH.

In this section, we briefly discuss CMP materials for photocatalytic H_2 evolution from water splitting with quite a few excellent examples. The quintessential CMPs for photocatalytic H_2 evolution from water splitting and their BET surface area, pore-volume, and H_2 evolution related properties are summarized in Table 1.[89,104,105,126–138]

As early as 1980, it was reported that porous polymers were used for H_2 evolution, which did not attract much attention. Subsequently, until Mullen's group were found 3D conjugated poly(azomethine) networks to be able to efficiently photocatalysis of H_2 evolution from water splitting in 2010,[139] and since then various CMPs have been developed to improve the efficiency of H_2 evolution. Cooper's group prepared a series of polyphenylene-based CMPs (CP-CMP1-15) with a tunable bandgap (Fig. 8a).[140] They found that CMPs made of different monomer components have different photophysical characteristics, which are promising photocatalysts for H_2 evolution from water splitting without an obvious need for additional cocatalyst. As shown in Fig. 8b and c, a regular redshift in the bandgap is observed with the increase of pyrene monomer content when growing CP-CMP1 to CP-CMP15. The modular chemical strategy

used to prepare these polymers is comparable to the synthesis of graphene nanomaterials.[141] This strategy helps to control the electronic structure and porosity of polymer materials, which will help to advance the design and synthesis of photocatalysts that are comprehensively used for water decomposition.

In a subsequent new study, they prepared a series of extended CMPs such as extended biphenyl CMPs (PE-CMPs), extended 1,3,5-linked CMPs (ME-CMPs), extended spirobifluorene CMPs (ESP-CMPs) to study the important photocatalytic properties (*e.g.* the geometry of the skeleton, the length of the comonomer, and the degree of planarization of the linker) of these CMPs for photocatalytic production of hydrogen from water splitting.[142] These results and previously reported other findings[78,99,143] show that CMP materials have the potential for photocatalytic HERs, but there are differences in effect. Fig. 9a shows the structures of these CMPs. A red-shifted absorption in the solid-phase UV-visible spectrum occurs from CP-CMP1 to PE-CMPs (Fig. 9b). They all can act as photocatalysts for hydrogen evolution (Fig. 9c and d). PE-CMPs and CP-CMP1 are not ideal for hydrogen production under visible light. The hydrogen production rate of PE-CMPs (716 μmol h^{-1}

This journal is © The Royal Society of Chemistry 2020

J. Mater. Chem. A, 2020, **8**, 6434–6470 | **6441**

Table 1 Summary of the BET surface area, pore volume, and H$_2$ evolution related properties of quintessential CMP photocatalysts

CMPs	Molecular structure	Band gap [eV]	HOMO/LUMO [eV]/[eV]	S_{BET} [m^2 g^{-1}]	V_{total} [cm^3 g^{-1}]	Pore size [nm]	Cocatalyst (wt%)	Sacrificial agent	Light source[a]	HER[b] [μmol h^{-1} g^{-1}]	AQY[c] [%]	Ref.
PrCMP-1		1.74	+0.65/−1.09	558	0.36	—	—	TEOA	>300 nm	371	—	89
PrCMP-2		1.61	+0.56/−1.05	820	0.60	—	—	TEOA	>300 nm	938	—	89
PrCMP-3		1.53	+0.50/−1.03	972	0.66	—	—	TEOA	>300 nm	1210	—	89
COP-TP		2.85	+1.46/−0.39	640	—	3–6	—	TEOA	≥400 nm	4200	1.5	104
Ta-CMP		2.90	−5.03/−1.85	423	—	—	—	TEOA	>420 nm	487	0.12	126
Ta-CMP-N		2.90	−4.99/−1.80	408	—	—	—	TEOA	>420 nm	99	0.07	126
Ta-CMP-CN		2.88	−5.10/−1.90	398	—	—	—	TEOA	>420 nm	698	0.15	126
L-PyBT		2.23	+1.43/−0.80	13–47	—	2.0–17	—	TEOA	>420 nm	1674	—	127
L-PyDFBT		2.28	+1.44/−0.84	13–47	—	2.0–17	—	TEOA	>420 nm	418	—	127
P-PyBT		2.07	+1.23/−0.84	151	—	2.0	—	TEOA	>420 nm	6	—	127
P-PyDFBT		2.19	+1.32/−0.87	499	—	2.0	Pt (3.0)	TEOA	>420 nm	30	—	127

Table 1 (Contd.)

CMPs	Molecular structure	Band gap [eV]	HOMO/LUMO [eV]/[eV]	S_{BET} [m² g⁻¹]	V_{total} [cm³ g⁻¹]	Pore size [nm]	Cocatalyst (wt%)	Sacrificial agent	Light source[a]	HER[b] [μmol h⁻¹ g⁻¹]	AQY[c] [%]	Ref.
PCTF-8		2.25	—	625	0.32	—	Pt (2.3)	TEOA	≥400 nm	118.5	—	128
4-CzPN		2.11	+1.30/−0.81	692.45	0.32	—	Pt (3.0)	TEOA	≥400 nm	2103.2	6.4	129
CTF-2		2.73	—	—	—	—	Pt (3.0)	TEOA	>420 nm	296 ± 11	1.6	130
P16PySO		2.31	+1.25/−1.06	—	—	—	Pt (3.0) — Pt (3.0) —	TEOA TEOA	>300 nm >420 nm	15 480 8100 11 200 6380	— — — —	131
P27PySO		2.48	+1.44/−1.04	—	—	—	Pt (3.0) — Pt (3.0) —	TEOA TEOA	>300 nm >420 nm	5640 4720 1780 1400	— — — —	131
P1		2.3	+1.91/−0.42	—	—	2	Pt (3.0)	TEOA	≥420 nm	1000	3.58	132
P2		3.9	+2.50/−0.44	—	—	2	Pt (3.0)	TEOA	≥420 nm	Trace	0.23	132
CP1		1.79	+0.96/−0.83	251.3	—	—	Pt (0.5) —	AA/DMF	>420 nm	30 810 15 975	1.62[d]	105
ter-CTF		2.11	+1.35/−0.76	586	—	—	Pt (1.95)	TEOA	≥420 nm	19 300	22.8	133
Tr-F3N		2.37	+1.03/−1.34	105	—	10–50	—	EG/TEOA	>300 nm	538	—	134
S-CMP3		2.56	—	523.8	—	—	Pt (3.0)	TEA/MeOH	>420 nm >295 nm	3106 6076	13.2	135
CTF-N		2.17	+2.09/−0.38	650	—	—	Pt (2.1)	TEOA	>420 nm	538	4.07	136

This journal is © The Royal Society of Chemistry 2020

J. Mater. Chem. A, 2020, 8, 6434–6470 | 6443

Table 1 (*Contd.*)

CMPs	Molecular structure	Band gap [eV]	HOMO/LUMO [eV]/[eV]	S_{BET} [m^2 g^{-1}]	V_{total} [cm^3 g^{-1}]	Pore size [nm]	Cocatalyst (wt%)	Sacrificial agent	Light source[a]	HER[b] [µmol h^{-1} g^{-1}]	AQY[c] [%]	Ref.
OB-POP-3		2.14	1.52/−0.62	834	—	50	Pt (3.0)	TEOA	>420 nm >295 nm	908 1322	2.0	137
SNP-2		—	—	370	0.33	—	Pt (3.0)	TEOA	395 nm	472	—	138

[a] 300 W Xe-Lamp. [b] Maximum HER. [c] AQY at 400 nm. [d] AQY at 550 nm; AQY: apparent quantum yield; TEOA: triethylamine; DMF: *N,N*-dimethylformamide; AA: ascorbic acid; EG: ethylene glycol; TEA: trimethylamine.

g^{-1}) is higher than that of CP-CMP1 (164 µmol h^{-1} g^{-1}) under UV/visible light (>295 nm). SP-CMPs showed the highest photocatalytic activity and the highest specific surface area. It exhibited the highest hydrogen production rate (1152 µmol h^{-1} g^{-1}) under broadband illumination (>295 nm). However, the general correlation between the porosity of SP-CMP and photocatalytic performance has not been found, which requires further investigation and needs more methods for increasing the photocatalytic activity.
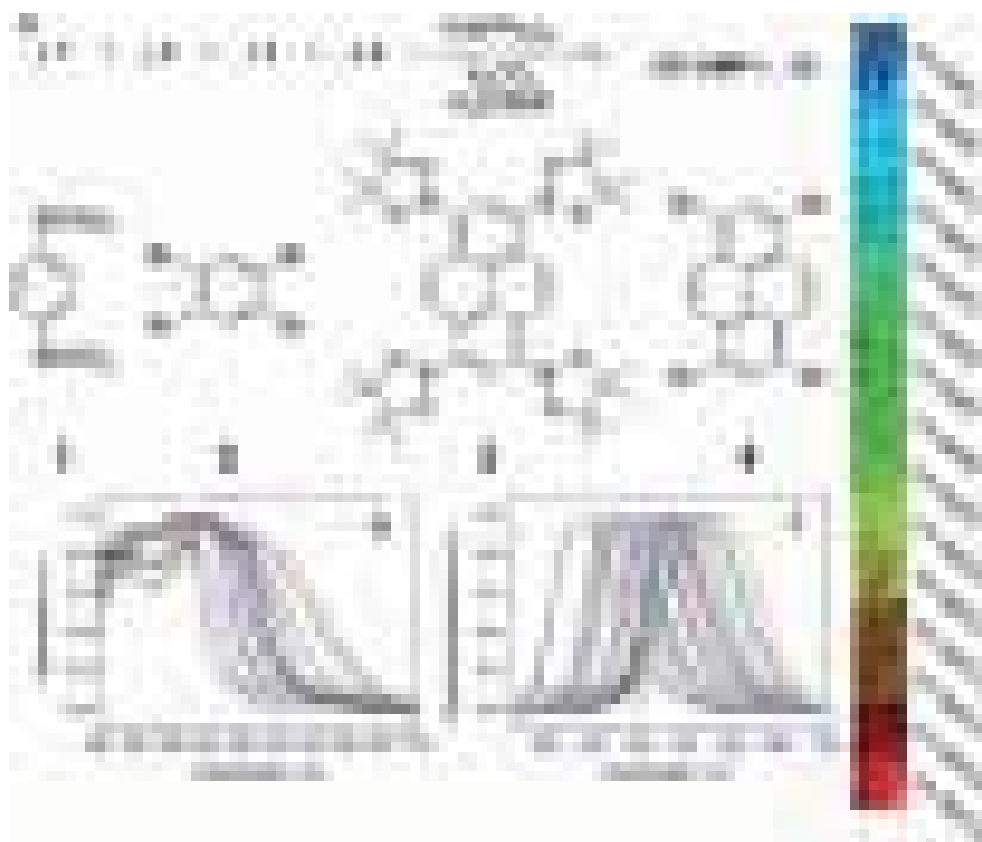

Fig. 8 (a) Synthesis of CP-CMP1-15 by Suzuki−Miyaura polycondensation. The photophysical properties of these CMP photocatalysts tuned by statistical copolymerization. (Photographs in the right) CP-CMP1−15 imaged under irradiation with UV light ($\lambda_{excitation}$ = 365 nm). (b) UV-visible absorption spectra and (c) photoluminescence spectra of these polymers recorded in the solid state. Reprinted with permission from ref. 140. Copyright 2015 American Chemical Society.
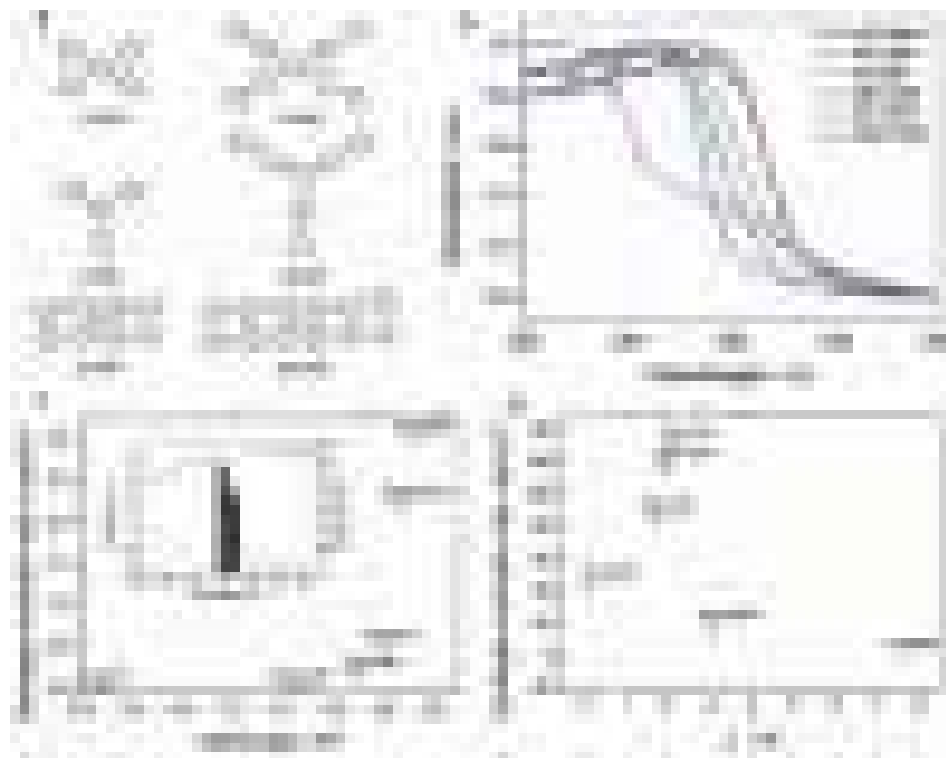
6444 | *J. Mater. Chem. A*, 2020, **8**, 6434–6470

This journal is © The Royal Society of Chemistry 2020

Fig. 9 (a) Structures of CMPs. (b) UV/vis reflectance spectra of CMPs in the solid-state. (c) H_2 evolution rates under visible light ($\lambda > 420$ nm) correlated with the band gap of CMPs. (d) Correlation of the life-time of the excited state with H_2 evolution rates under broadband illumination ($\lambda > 295$ nm). Reprinted with permission from ref. 142. Copyright the Royal Society of Chemistry 2016.

The introduction of precious metal nanoparticles into CMP networks helps to enhance the overall photocatalytic efficiency of these photocatalysts for H_2 evolution from water splitting. As an example, Inagaki reported that a 9,9'-spirobifluorene-based CMP loaded with Pt metal (Pt/COP-3) has a higher rate of hydrogen production than COP-3.[144] COP-3 is an organic polymer having a large specific surface area and a large micropore volume.[145] The HOMO and LUMO levels of COP-3 are enough to oxidize TEOA and reduce H^+. Direct loading of Pt onto COP-3 can be beneficial to increase the transfer of photogenerated electrons and thereby increase the photocatalytic activity to increase the photocatalytic performances of composite photocatalysts. Recently, a series of Py-based CMPs have been produced by a direct C–H arylation coupling reaction for the first time.[105] Among them, four-directional pyrene–bithiophene-based CMP (CP1) has photocatalytic HERs of 15 975 µmol h^{-1} g^{-1} under visible light with AA/DMF/H2O as sacrificial agent without Pt cocatalyst. The HERs is nine times higher than that of the previously reported organic photocatalyst under the same conditions (1773.3 µmol h^{-1} g^{-1}). It is worth noting that its hydrogen production rate reached an attractive 30 810 µmol h^{-1} g^{-1} after encapsulating a 0.5 wt% Pt co-catalyst. Meanwhile, it should also be noted that the presence of DMF is different from the commonly used MeOH sacrificial agents. The non-covalent interaction of hydrogen bonds between DMF and H_2O contributes to the separation of photogenerated charge carriers. This strategy is a preliminary, simple and attractive new method

to enhance the photocatalytic activity by adjusting the reaction matrix, and its mechanism needs further systematic research.

Jiang *et al.* found that the physicochemical properties (*e.g.* pore structure and bandgap) of CMPs could be adjusted by changing the type and position of the substituents. As shown in Fig. 10, a series of perylene-containing CMPs (PrCMPs)[146,147] and a series of dibenzothiophene dioxide containing CMPs (DBTD-CMPs)[148] have been synthesized by using the Suzuki–Miyaura reaction. The BET surface area of PrPy is higher than that of PrTPE, which is 1219 m^2 g^{-1} and attributed to its rigid polymer backbone from planar pyrene units. The physicochemical properties (*e.g.* pore structure and bandgap) of PrCMPs can be adjusted by changing the type and position of the substituents to obtain optimal photocatalytic properties. The photocatalytic HERs results showed that Pr-CMPs have better photocatalytic performances, which are due to their high conjugated, high specific surface area, a wide range of light absorption, low photoluminescence lifetime, and planar structure. The geometry of the linker plays a key role in enhancing the photocatalytic activity of CMP materials. Meanwhile, the crosslinker length has an effect on photocatalytic hydrogen production. The results indicate that short benzene crosslinkers will be more conducive to improving the photocatalytic activity of DBTD-CMPs. This is because the reduction of the length of the cross-linking agent reduces the degree of conjugation and planarization of the CMP molecules, thereby promoting the transport and separation of light-induced charge carriers.

Fig. 10 Chemical structures of PrCMPs and DBTD-CMPs for photocatalytic H_2 evolution reactions (HERs).

Attractively, the DBTD-CMP1 loaded Pt metal showed remarkable high HER (9200 μmol h^{-1} g^{-1}) under broad band UV-vis light radiance and high AQY (3.3%) at 400 nm. These studies show that these CMP organic photocatalysts have prospects for photocatalytic HERs and provide useful guidance for the rational design of these polymers.

In order to accelerate the research and search for excellent performance CMP photocatalysts for H_2 evolution from water splitting, the strategy of combining experiments with theoretical simulations, intelligent robotics, and other new technologies can be considered. As one of the pioneers in the field of CMP materials, Cooper and collaborators studied the relationship between the structure of these polymers and their photocatalytic properties for HERs by combining high-throughput calculations and robotic experiments.[149] They use this strategy to systematically build a database of CMP photocatalysts for H_2 evolution from water splitting. In this database, the machine learning model uses four variables (such as electron affinity, ionization potential, bandgap, and polymer particle dispersion in solution) with high correlation to describe the photocatalytic performance of different polymers. Fig. 11a shows the workflow for the synthesis and screening of polymer libraries, and the effective comonomers used in the research to synthesize polymers. In the calculation and test, they considered a total of 6354 copolymers, and synthesized and characterized sub-libraries of more than 170 copolymers. Fig. 11b shows the optical properties of the 6354 copolymers in the entire polymer library. They predicted and tested these polymers for photocatalytic hydrogen production and found that all materials have photocatalytic activity for hydrogen production with HER rates ranging from 36.8 to 9828 μmol g^{-1} h^{-1}. Their results show that

there is a weak link between the activity of photocatalytic HERs and every property of the polymer, which supports the opinion that the factors affecting photocatalytic HERs are multifactorial properties that are related to many mutually independent factors.

3.2 CMPs for photocatalytic O_2 evolution reactions

The other half of the water-splitting reaction, also known as the oxygen evolution reaction (OER), is one of the main challenges for the convenient and widespread production of hydrogen from water. The formation of photocatalytic molecular oxygen (O_2) involves a complex multi-electron transfer process, which is an uphill process with a large overpotential and a slow kinetic process.[150–152] Furthermore, it may be useful to study the formation of H_2 and the fixation of CO_2 by the photocatalytic OER process because the electrons and protons released during the production of O_2 by water splitting have an important role in the formation of H_2 and the fixation of CO_2.[153] This makes the development of feasible and efficient photocatalytic OER catalysts a challenging and urgent task. To date, the most common OER catalysts are noble metal-based materials, which have limited reserves and high cost. An attractive approach is to use abundant elements on the planet to develop low-cost and high-performance catalysts for OERs.

CMPs have adjustable photoelectric and structural properties and are emerging photocatalysts for OERs. In order to enhance the reactivity of photocatalytic OERs, poly(1,3,5-triethynylbenzene) (PTEB)[154] and 2D aza-fused CMPs[155] have been used to improves the OER kinetics. Fig. 12a and b show the synthesis and chemical structure of these CMPs. The energy
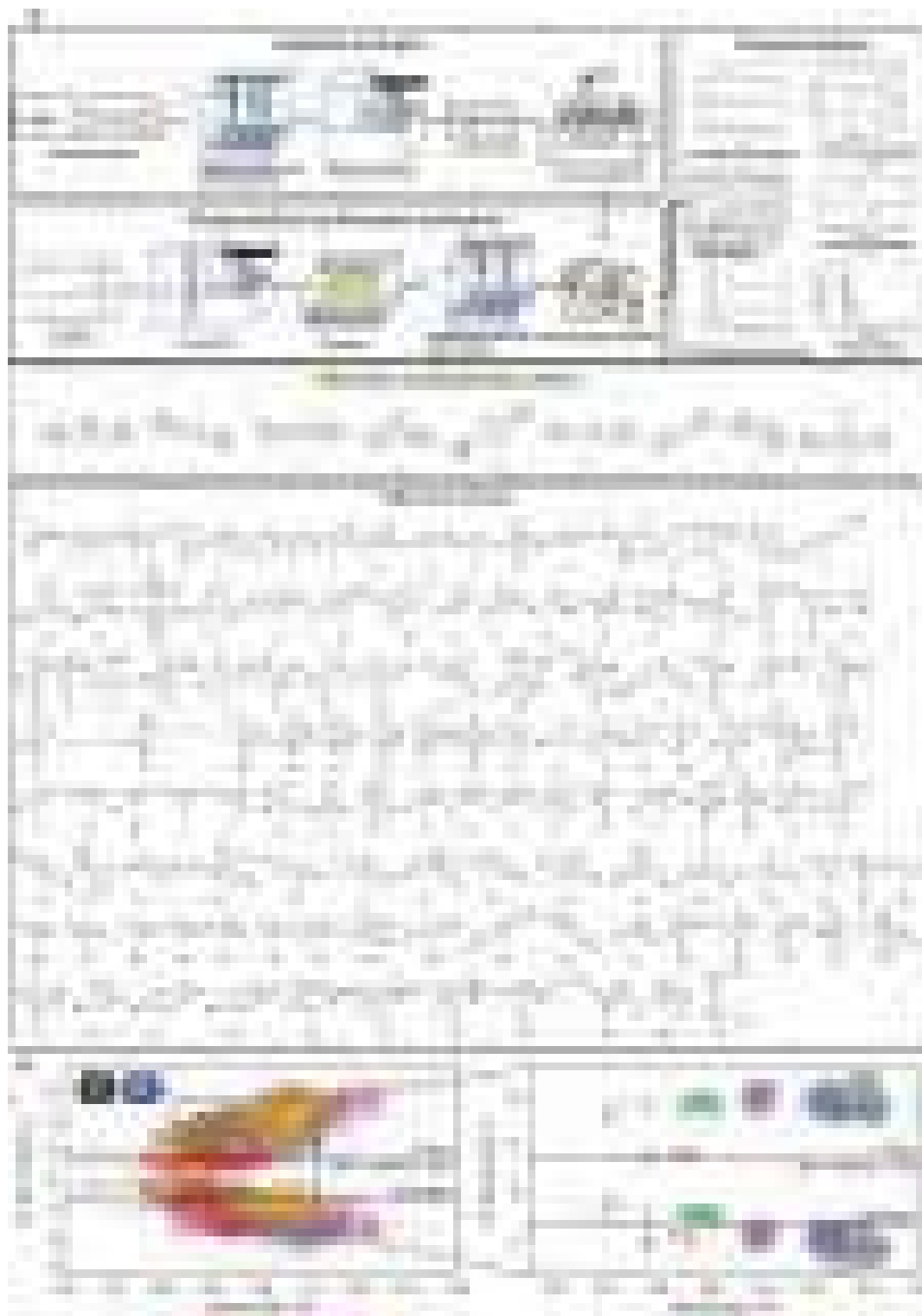
Fig. 11 The combination of experiment and theory for faster finding of polymer photocatalysts for H$_2$ evolution from water splitting. (a) The workflow of the synthesis and screening of polymer libraries, diboronic acids/acid esters and dibromo monomers used to synthesize the copolymers in the photocatalyst libraries; (b) predicted electron affinity (EA), predicted ionization potential (IP), and predicted optical gap of the entire 6354 co-polymers formed by the exhaustive combination of the compounds outlined in (a). Reprinted with permission from ref. 149. Copyright 2019 American Chemical Society.

level of PTEB and aza-CMP films is beneficial to promote water oxidation under neutral and alkaline conditions (Fig. 12c and d). Remarkably, the bandgap of CMPs decreases from 1.65 eV to 1.26 eV as the number of layers increases from 1 to 4. First-principles calculations show that aza-CMP films have the potential to catalyze OERs using visible and near-infrared light.
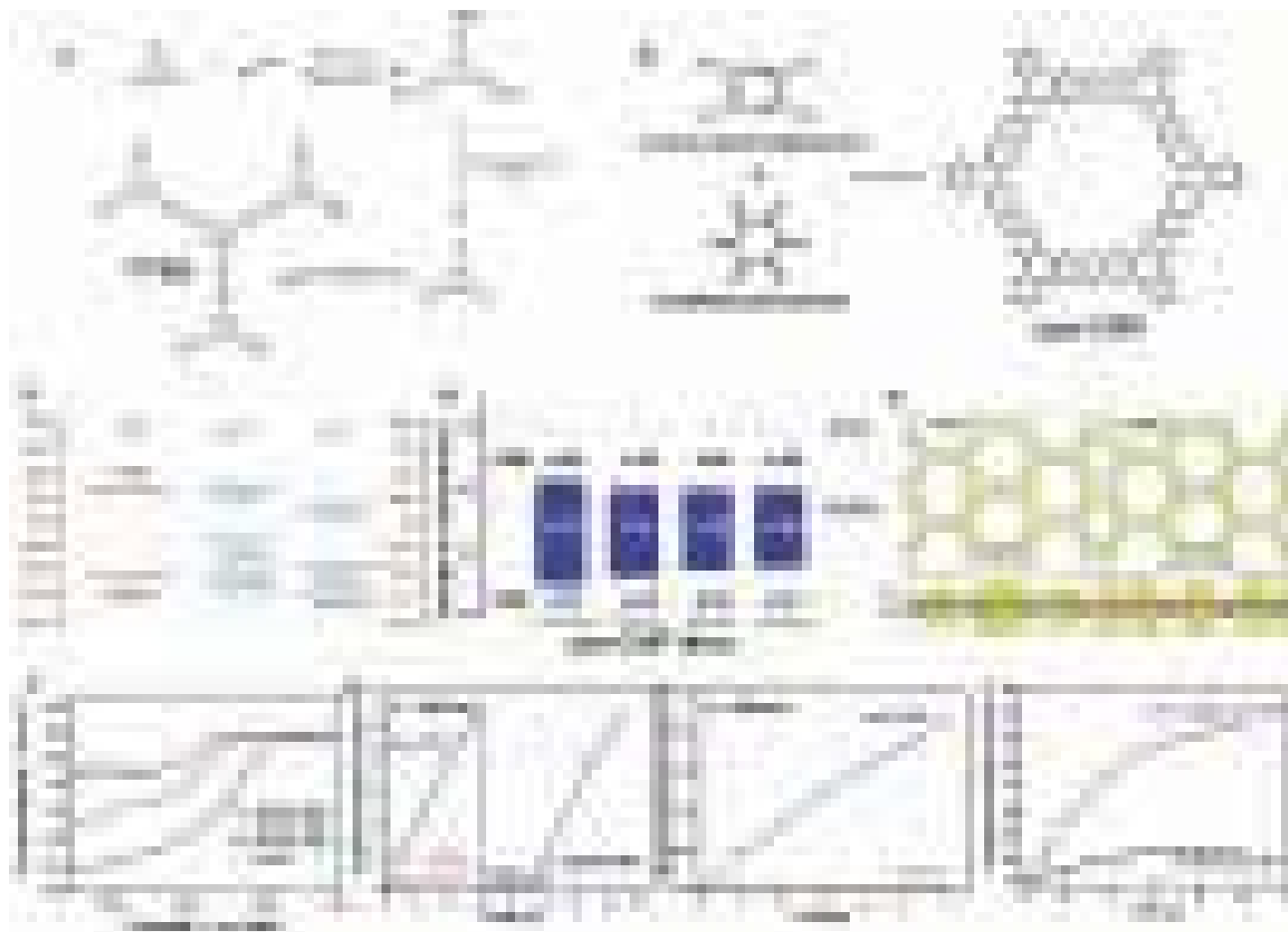
This journal is © The Royal Society of Chemistry 2020

J. Mater. Chem. A, 2020, **8**, 6434–6470 | **6447**

Fig. 12 The representative CMPs for photocatalytic oxygen reduction reactions. (a) The synthesis and chemical structure of (a) PTEB and (b) aza-CMP; (c) the band gap of PTEB and the energy levels of water oxidation and reduction at pH 7 and 13; (d) the change of the VBM and CBM of aza-CMP films with the layer number; (e) the charge density distributions of the CBM and VBM at the Γ k-point for an ideal single-layer aza-CMP nanosheet; (f) linear sweep voltammograms of undoped and N-doped PTEB recorded at a rotation rate of 1600 rpm and scan rate of 5 mV s^{-1}; representative time course of O_2 evolution by using the aza-CMP films under (g) visible light and (h) NIR light illumination; (i) representative time course of O_2 evolution under visible light irradiation by using the exfoliated ultrathin aza-CMP films and Co(OH)$_2$-loaded aza-CMPs, respectively. (a), (c) and (f) Reprinted with permission from ref. 154. Copyright 2017 Wiley-VCH; (b), (d), (e), (g), (h) and (i) Reprinted with permission from ref. 155. Copyright the Royal Society of Chemistry 2017.

These charge density diagrams of the valence band maximum (VBM) and the conduction band minimum (CBM) (Fig. 12e) further confirm that their highly conjugated structures are conducive to the effective migration of photogenerated electrons to enhance the photocatalytic activity for OERs. The linear sweep voltammograms (Fig. 12f) support one opinion that nitrogen-doped PTEB (NPTEB) has better catalytic activity than undoped PTEB. The increase in the catalytic activity of NPTEB may be attributed to: (i) an increase in the number of electrochemically active sites; (ii) an increase in pore size; and (iii) an increase in the hydrophilicity of the material, which is important for aqueous reactions. As shown in Fig. 12g, the average OER rate of aza-CMP films can reach about 1.0 μmol h^{-1} in the presence of electron acceptors under visible light, which exceeds that of the g-C$_3$N$_4$ photocatalyst (0.12 μmol h^{-1}). Meanwhile, Fig. 12g show that the O$_2$ production rate of regenerated aza-CMP film are maintained at the initial value which indicate the stability of aza-CMP for photocatalytic OERs.

Furthermore, aza-CMP is the first metal-free photocatalyst that has been shown to promote OERs ($\sim$0.4 μmol h^{-1}) under NIR spectral light ($\lambda > 800$ nm), while g-C$_3$N$_4$ is inactive (Fig. 12h). Remarkably, as shown in Fig. 12i, the OER rate of the 3 wt% Co(OH)$_2$-loaded aza-CMP film increased vastly to 14.3 μmol h^{-1} under visible light, which is four times that of the original aza-CMP film. This inspires us to develop forms other than amorphous powders of CMP materials.

3.3 CMPs for photocatalytic overall water splitting

Photocatalytic water overall splitting can efficiently produce hydrogen and oxygen from water under direct sunlight without a sacrificial agent compared to water splitting half-reacting HERs and OERs.[156–161] Current common photocatalysts for overall water splitting still have disadvantages such as instability, low quantum yield, and unregulated optoelectronic and structural properties.[112,162–165] Inspired by these challenges of

developing high-performance photocatalysts for overall water splitting, scientists have developed simple conjugated polymers with earth-rich elements for low-cost, efficient and stable photocatalysts for water splitting.[166] However, the challenge is not so easy to overcome. These polymers lose their activity in overall pure water splitting because of the unsuited bandgap, slower separation and migration of photo-generated carriers, and the lack of surface redox sites.[140,167–170] As an example, although g-C_3N_4 has been widely used in the water splitting half-reaction (HER), it loses activity in the overall pure water splitting reaction.[171–173] In particular, these polymers require a large number of sacrificial agents for photocatalytic H_2 evolution from water splitting, which is not conducive to universal application. Therefore, since the development of these polymer materials science, polymer photocatalysts developed for overall water splitting under visible light in the absence of sacrificial agents have been pursued by scientists in materials science and solar energy conversion engineering.

As an excellent material platform, CMPs can be used for the design of photocatalysts with high catalytic stability and high photocatalytic activity for overall water splitting under visible light. Compared to other conventional photocatalysts, CMPs composed of a π-conjugated system have excellent chemical stability and thermodynamic stability. Meanwhile, the electron band structure of the benzene ring of the monomer of CMPs has the function of rotation. By changing the dihedral angle between adjacent benzene rings, the structure of CMP materials can be optimized to make them more stable at the energy level. It is well known that the modification of the material morphology, such as ultrathin sheet structures, allows the photoexciton to reach the polymer surface quickly, thus inhibiting the recombination of photogenic electron hole pairs and improving the photocatalytic activity of the material.[174,175] The morphology of CMPs can be adjusted by adjusting the type of reaction, reaction conditions, and monomer types. Furthermore, the band gaps of CMPs can be adjusted by band gap engineering so that the CMPs have a suitable band gap to absorb visible photons, and their band edge potential can span the reduction potential and oxidation potential of water.

For the first time, 1,3-diyne-linked CMP nanosheets (CMPNs) have been synthesized by an oxidative coupling reaction and are applied to photocatalytic overall pure water splitting under visible light.[176] The as-prepared CMPNs with 1,3,5-tris-(4-ethynylphenyl)-benzene (TEPB) and 1,3,5-triethynylbenzene (TEB) by oxidative coupling (Fig. 13a) exhibit a sheet-like structure with 614 and 630 m^2 g^{-1} BET surface areas and 1.9 and 3.2 nm average pore sizes, respectively. Fig. 13b shows that the unique charge distribution characteristics of the VBM and CBM of PTEPB and PTEP are conducive to the rapid and efficient transport of photogenerated electrons and holes for water splitting. In the terms of energy, the buckling structure of PTEPB is more stable than the flat structure of PTEPB. Meanwhile, this work found that CMPNs remained highly catalytically stable after 48 hours of repeat visible light catalytic experiments, suggesting that CMPNs can reduce surface charge accumulation and prevent harmful photochemical degradation. The results of thermogravimetric analysis of two kinds of CMPNs in air show that both PTEPB and PTEB have thermal stability. C 1s XPS spectra and TEM images confirm that the CMP structure is highly stable. Furthermore, carbon–carbon triple bonds of the 1,3-diyne covalent linkage are Raman active,[177] which introduced into the CMP networks can notably reduce the optical gap (from 4.62 to 3.04) to enhance photocatalytic performances for overall water splitting. PTEPB and PTEP catalyze water splitting for the simultaneous generation of H_2 and O_2 under the irradiation of light, and the production ratio is very close to the stoichiometric ratio of H and O in water molecules. The AQY of PTEPB and PTEP for overall water splitting reaches 7.6–10.3% under visible light. This is even higher than that of existing noble metal loaded photocatalysts.[178] This whole reaction process of water splitting by using these polymers is proved by the results of theoretical simulation, which indicated that these CMPNs have multiple reaction sites for the overall water splitting reaction, which can photocatalyze a pure water (pH ≈ 7) splitting reaction by a four-electron pathway under visible light (Fig. 13c). This provides a feasible strategy for the development of low-cost and efficient photocatalysts for direct overall water splitting under sunlight without additional input.

4. CMPs for photocatalytic CO_2 reduction reactions

Besides photocatalytic water splitting, capturing and converting CO_2 as a part of artificial photosynthesis is also a sustainable solution to energy and environmental issues as well as mitigating global warming.[179] Using artificial supramolecular structures to stimulate artificial photosynthesis for converting CO_2 into sustainable fuels by using solar energy is a promising strategy, yet a formidable challenge. Their advantages include mild operating conditions, abundant and cheap raw materials, and high-value products. Meanwhile, their challenges are that few materials can overcome the high bond energy (~750 kJ mol^{-1}) of CO_2 and efficiently convert CO_2.[180] Previous research reports briefly described the basic concepts and principles of photocatalytic reduction of CO_2 under sunlight, and emphasized the shortcomings of low light energy conversion efficiency and poor selectivity of existing photocatalytic materials.[119,181–184] In order to deal with these challenges, it is suggested to design a highly active catalytic system from the four aspects, such as the adsorption of reactants, the separation and transfer of charges, the collection of light, and the activation of CO_2. The available strategies include:[184] (i) effective adjustment of the band gap and band position of material molecules; (ii) material nano-crystallization for rapid separation and transfer of photo-generated electron pairs; (iii) improvement of the surface properties of materials for CO_2 adsorption and activation; (iv) the formation of channels in the structure, which increases the surface area of photocatalysts for increasing the adsorption of reactants and providing more surface-active sites; (v) exposure facet engineering for adjusting the electronic band structure; (vi) development of composite photocatalysts for effective reduction of the activation barrier of CO_2; (vii)
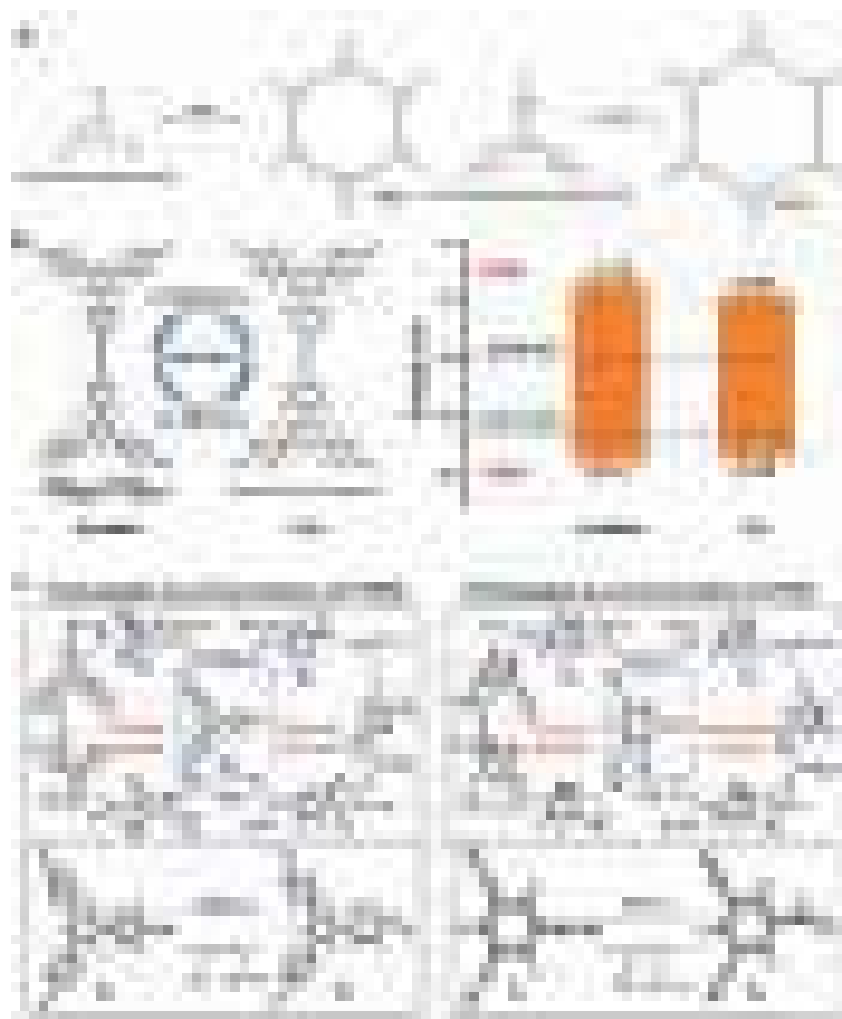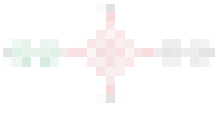
This journal is © The Royal Society of Chemistry 2020

J. Mater. Chem. A, 2020, **8**, 6434–6470 | **6449**
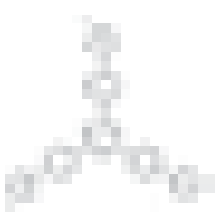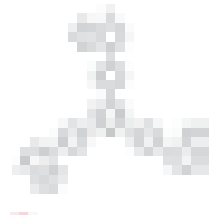
Fig. 13 (a) Synthetic and chemical structures of PTEB and PTEPB; (b) the optimized structures of buckled and flat PTEPB with the corresponding energy positions of the VBM and CBM; (c) proposed photocatalytic cycles of oxygen evolution reactions (*via* single-site and dual-site processes) and HERs with the energetically most feasible active sites in both PTEPB and PTEB. S_0 is the bare surface. S_x^s ($x = 1, 2, 3$) and S_x^d ($x = 1, 2, 3, 4$) are the structures of intermediate states involved in oxygen evolution reactions *via* single-site and dual-site catalytic processes, respectively. Red, gray, and white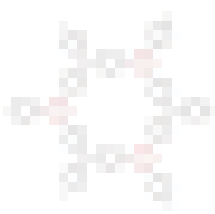 balls represent oxygen, carbon, and hydrogen atoms, respectively. Reprinted with permission from ref. 176. Copyright 2017 Wiley-VCH.

development of Z-scheme photocatalytic systems for promoting surface chemical reactions and inhibiting reverse redox reactions. Nowadays, CMPs as emerging and promising photocatalytic materials get the attention of the public.[185] Combining some CO_2 activation methods[186–188] with the adjustable properties of CMPs is expected to provide a new solution for photocatalytic CO_2 reduction. Table 2 gives the summary of the state-of-the-art development of CMPs for photocatalytic CO_2 reduction, including their molecular structure, photoelectric properties, pore properties, photocatalytic properties, and so on.[189–192]

Porphyrin tetracyclic compounds, as important compounds in the process of life evolution, are widely used in artificial light energy conversion systems.[193–195] Among them, metalloporphyrin derivatives can be used for photocatalytic CO_2 reduction.[196–199] Moreover, 2D polymers expose more active sites and have higher photocatalytic efficiency.[200–202] Taking into

account the advantages of 2D CMPs, the photocatalytic activity of metalloporphyrin derivatives for CO_2 reduction, and the dye-sensitizing effect of thiophenes, metal-modified 2D metalloporphyrin CMPs can be used to improve the ability of photocatalytic reduction of CO_2. These CMPs are constructed by introducing a series of metal atoms (Fe, Mg, *etc.*) into a novel thiophene-linked porphyrin polymer center, which can improve the electronic properties of these polymers, thereby promoting the CO_2 reducing ability.[203] The research presented that iron-modified CMPs have the highest CO_2 reduction capacity, which may be attributed to their unique semi-metallic properties and band structure. The intermediates involved in CO_2 reduction are shown in Fig. 14a, and the reaction steps and activation energy (E_a) of various species involved in the CO_2 reduction process are shown in Fig. 14b. In the carboxyl pathway, CO_2 is finally reduced to CH_4, and the by-product is HCOOH, which is the preferred thermodynamic reduction

6450 | *J. Mater. Chem. A*, 2020, **8**, 6434–6470

This journal is © The Royal Society of Chemistry 2020

Table 2 Summary of photocatalytic CO_2 reduction using quintessential CMPs

CMPs	Chemical structure	Band gap [eV]	HOMO/LUMO [eV]/[eV]	S_{BET} [m^2 g^{-1}]	V_{total}[a] [cm^3 g^{-1}]	Cocatalyst (wt%)	Main products (highest yield)	Selectivity [%]	Ref.
BpyMP-1		2.52	—	680 ± 30	0.50	Cp*Rh (1.6)	HCOOH, HCOONH$_4$ (TOF: 23.46 ± 0.69 h^{-1})	—	189[b]
BpyMP-2		2.55	—	970 ± 70	0.79	Cp*Rh (1.6)	HCOOH, HCOONH$_4$ (TOF: 22.49 ± 1.39 h^{-1})	—	189[b]
CMP-B		2.93	+1.81/−1.12	409	—	—	CO/H$_2$ (266.67 μmol h^{-1} g^{-1}/ 133.33 μmol h^{-1} g^{-1})	66.7	190[c]
CMP-Th		2.43	+1.42/−1.01	52	—	—	CO/H$_2$ (666.67 μmol h^{-1} g^{-1}/ 200 μmol h^{-1} g^{-1})	76.9	190[c]
CMP-BT		2.24	+1.31/−0.93	37	—	—	CO/H$_2$ (1213.33 μmol h^{-1} g^{-1}/ 273.33 μmol h^{-1} g^{-1})	81.6	190[c]
PEosinY-1		5.46	−7.01/−1.55	445	—	—	CO/H$_2$ (33 μmol h^{-1} g^{-1}/ 2 μmol h^{-1} g^{-1})	92	191[d]
PEosinY-2		5.55	−6.82/−1.26	131	—	—	CO/H$_2$ (26 μmol h^{-1} g^{-1}/ 4 μmol h^{-1} g^{-1})	—	191[d]
PEosinY-3		5.73	−7.20/1.47	610	—	—	CO/H$_2$ (12 μmol h^{-1} g^{-1}/ 30 μmol h^{-1} g^{-1})	—	191[d]
DA-CTF		2.35	—	715	0.35	1.2	CO/H$_2$/CH$_4$ (155 μmol h^{-1} g^{-1}/ 70 μmol h^{-1} g^{-1}/trace)	24.5	192[e]

[a] Determined at $p/p_0 = 0.95$. [b] Acetonitrile–triethanolamine (CAN : TEOA, 5 : 1, v/v) solution containing 1 mM Ru(bpy)$_3$Cl$_2$ as a photosensitizer, and 4 h of irradiation [420 nm, 200 W Hg (Xe) lamp (Newport Research Arc Lamp)]. [c] CMP (15 mg), CoCl$_2$ (1 mmol), dipyridyl (5 mmol), solvent (5 mL, acetonitrile/water = 4/1), TEOA (1 mL), CO$_2$ (1 atm.), white light ($\lambda > 420$ nm), 30 °C and 1 h. [d] Polymer (10 mg) dispersed in EtOH (2 mL), a 300 W Xe lamp ($\lambda > 420$ nm, 10 h), 1 atm and 25 °C. [e] DA-CTF (30 mg), CoCl$_2$·6H$_2$O (3.0 μmol), 2,2′-bipyridine (0.1 mmol), CO$_2$ (1 atm), solvent (2 mL), TEOA (1 mL), and visible light irradiation [300 W Xe lamp (PLS-SXE300C), $\lambda \geq 420$ nm]. TEOA: triethylamine; TOF: turnover frequencies.
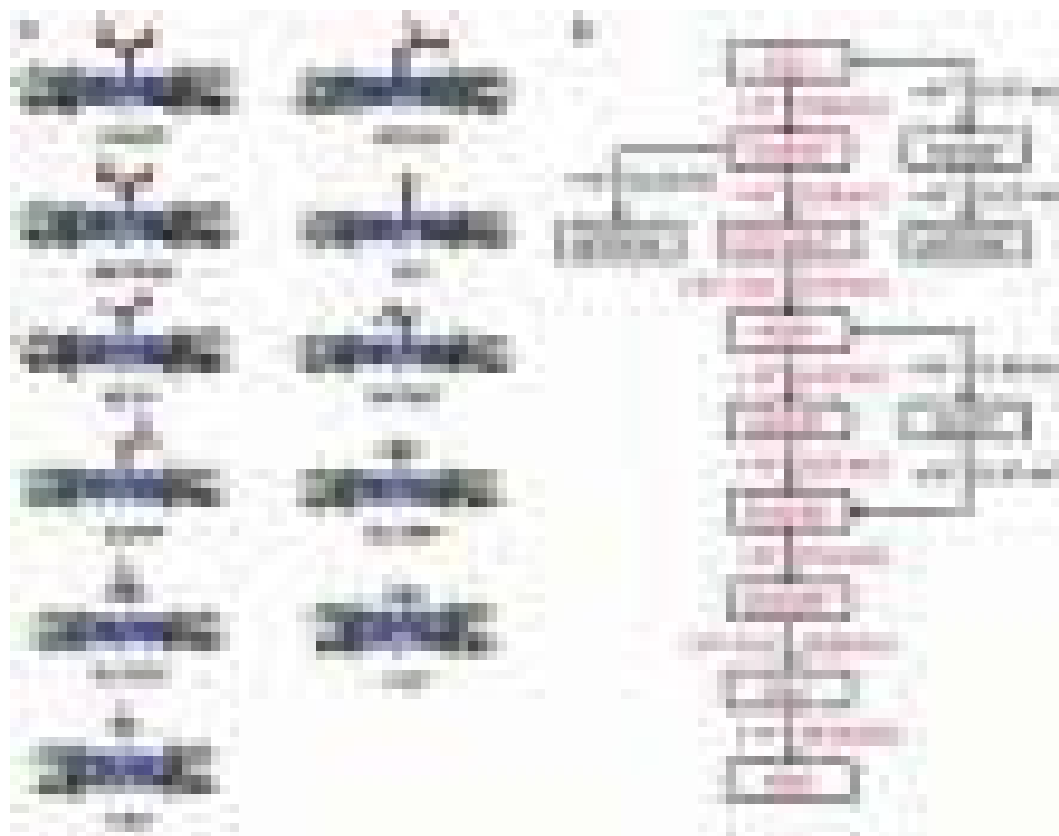
This journal is © The Royal Society of Chemistry 2020

J. Mater. Chem. A, 2020, **8**, 6434–6470 | **6451**

Fig. 14   (a) The optimized structures of each intermediate species involved in CO_2 reduction. (b) The overall pathway of CO_2 reduction and activation energy (E_a) of each basic step. Reprinted with permission from ref. 203. Copyright the Owner Societies 2018.

process. CH_4 is easily removed from the Fe-CMP substrate to vacate the reactive sites for other CO_2 molecules, facilitating the continued reduction of the reduction reaction. This outstanding research provides a new idea for the structural design of 2D metalloporphyrin CMP materials. Meanwhile, it provides a new path for photocatalytic reduction of CO_2.

Triazine-based CMP molecular networks can activate and reduce CO_2 under visible light because the substituent group (thiophene) on the triazine-based CMP backbone can promote charge separation.[190] These CMPs are synthesized by coupling various electron-donor and -acceptor monomers (Fig. 15a). The HOMO levels and the LUMO levels of these polymers can be adjusted by introducing different monomers (Fig. 15b), and the efficiency of photocatalytic CO_2 reduction can be improved by introducing different electron donor and electron acceptor groups. Among them, CMP-BT has the highest photocatalytic activity (CO/H_2: 1213.33 μmol h^{-1} g^{-1}/273.33 μmol h^{-1} g^{-1}) and stability (recycled 6 times) (Fig. 15c and d), and the results show that the selectivity of CMP-BT reached 81.6%, and the maximum AQY (at 405 nm) reached 1.75% (Fig. 15e).

As a robust platform, CMPs can be used to design photocatalysts with specific properties by changing the organic monomers and synthesis methods. For example, in order to control the selectivity of photocatalysts, researchers could consider using CO_2-philic monomers to construct CMP networks, which is helpful for efficient capture and further

highly selective conversion of CO_2. Recently, using this strategy, PEosinY-1 with a high BET surface area (610 m^2 g^{-1}) has been synthesized by coupling of Eosin-Y with 1,4-diethynylbenzene, which can efficiently promote photoreduction for conversion of CO_2 to CO (yield: 33 μmol g^{-1} h^{-1}) with the highest selectivity of 92% (Table 2) under visible light without any photosensitizer or sacrificial reagent.[191] Fig. 16 shows the possible mechanism for photocatalytic CO_2 reduction by using PEosinY-1. These outstanding contributions provide new horizons for the design and assembly of polymer-based photocatalysts for solar energy conversion with high performance.

5.   CMPs for photocatalytic organic conversion

Solar-driven organic conversion is a powerful tool for the synthesis of many important compounds. Photoactive transition metals (such as Ru, Ir, etc.) are some of the first materials for light-driven organic conversion. These materials have some inherent disadvantages such as high cost, low earth reserves, and lack of catalytic stability.[204–210] Therefore, the development of recyclable and metal-free high-efficiency heterogeneous catalysts for organic conversion remains a great challenge. In recent years, CMPs as a new class of recyclable metal-free photocatalysts have attracted great attention for photocatalytic
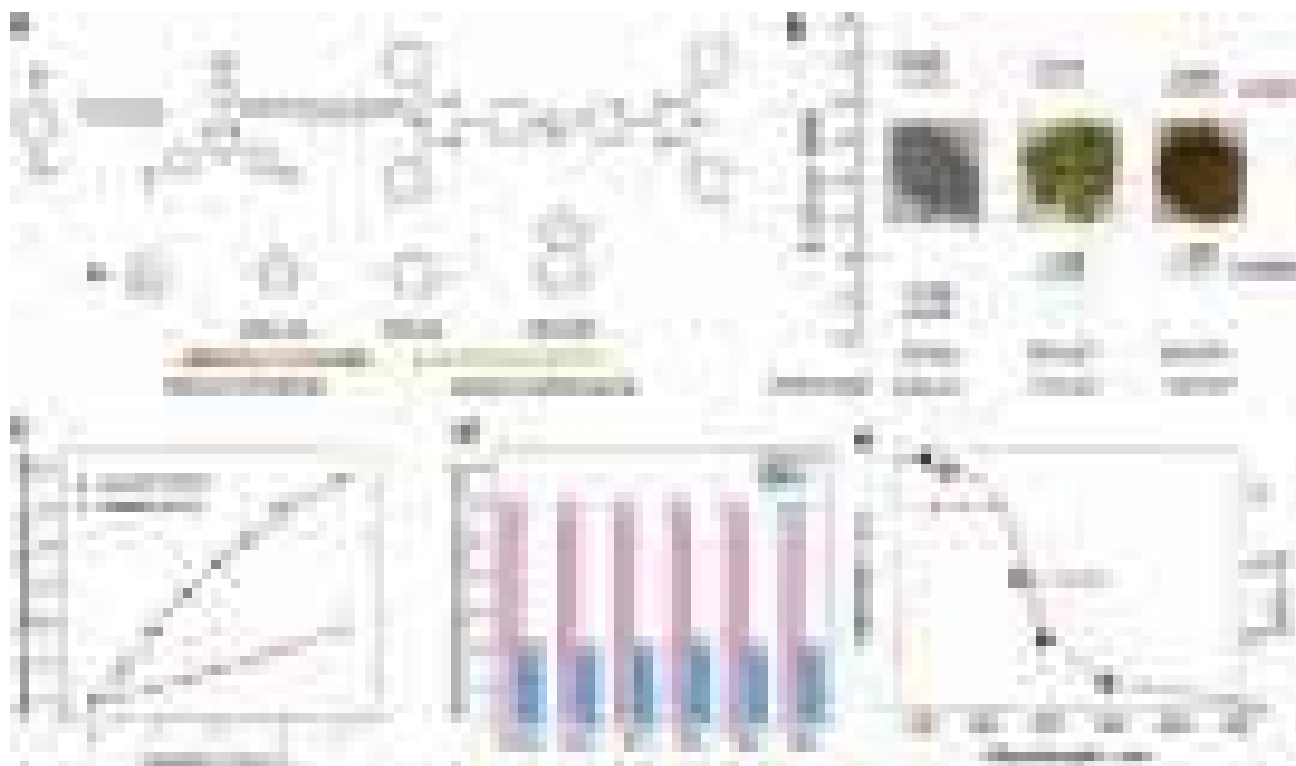
Fig. 15 (a) Illustrated design and synthesis pathway of three triazine-based polymers with different molecular structures for photocatalytic CO_2 reduction. (b) The HOMO/LUMO positions of the three CMPs and their matching photo. (c) Time dependence of CO and H_2 generation rates; reaction conditions: CMP-BT (15 mg), visible light irradiation ($\lambda > 420$ nm), and 4 h. (d) Stability and reusability tests of CMP-BT for CO_2 reduction. (e) Wavelength dependence of AQY for the H_2 and CO production at 405, 420, 470, 490, and 546 nm, respectively. TBPT-Br: 2,4,6-tris(4-bromophenyl)-1,3,5-triazine; B: 1,4-phenylenediboronic acid; Th: 2,5-thiophenediboronic acid; BT: 2,1,3-benzothiadiazole-,4,7-bis(boronic acid pinacol ester). Reprinted with permission from ref. 190. Copyright 2018 Wiley-VCH.

organic conversion owing to their high BET surface areas, high stability and adjustable functional.[211–215] Scientists have explored the photocatalytic performances of CMPs in organic conversion including α-alkylation of aldehydes, oxidative coupling of amines, hydroxylation of arylboronic acid, aza-

Fig. 16 Possible mechanism for photocatalytic CO_2 reduction by using PEosinY-1. Reprinted with permission from ref. 191. Copyright 2019 Wiley-VCH.

Henry reactions, and Stille-type coupling reactions (Table 3).[214,216–225]

Each monomer of CMP materials is connected by a conjugated bond, and they are synthesized by using silica as a template with high reaction conversion rates in organic conversion, but the efficiency and reaction rate are not high.[92] To solve this problem, the rigid structure of metallophthalocyanine-based CMPs (MPC-CMPs) can be considered.[226] The rigid porous structure of MPC-CMPs can effectively prevent the polymerization of MPC units, thereby increasing the chance of contact between the reactive sites and the reaction substrate. Moreover, BODIPY (4,4-difluoro-4-bora-3a,4a-diaza-sindacene) dye with high quantum yields and high photocatalytic stability[227–230] can be introduced into CMP networks and is beneficial to synthesis BODIPY-based CMPs (CMPBDPs) with good performance for organic conversion. There are two main methods for synthesizing CMPBDPs: (i) palladium metal-catalytic Suzuki–Miyaura coupling reaction and (ii) metal-free catalytic post-synthesis conversion method.[231] The BET surface area of the synthesized CMPBDP reached 484–769 m^2 g^{-1}. It has high stability, a high surface area and high efficiency heterogeneous photocatalytic activity in organic conversion, and it as a photocatalyst for the oxidation of thioanisole is four times faster than the corresponding soluble photocatalyst, and it can be cycled multiple times under visible

Table 3 Summary of CMPs as photocatalysts for organic conversion

CMPs	Chemical structure	Band gap [eV]	HOMO/LUMO [eV]/[eV]	S_{BET} [m^2 g^{-1}]	V_{total} [cm^3 g^{-1}]	Pore size (nm)	Light resource[a]	Reaction time [h]	Yield[b] [%]	Reused times	Ref.
Cz-POF-1		3.30	—	2065	—	—	LED	12	92	10	216
CF-HCP		2.25	+1.38/−0.87	1200	0.92	—	LED	6	>99	—	217
BBT@TiO$_2$		2.11	—	129	0.11	—	LED	6	98	5	218
P4-1		2.47	−6.06/−3.59	162.4	0.37	3.8	LED	5	>99	5	219
B-COP		—	—	—	—	—	LED	36	98	5	220

Table 3 (*Contd.*)
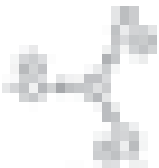
CMPs	Chemical structure	Band gap [eV]	HOMO/LUMO [eV]/[eV]	S_{BET} [m² g⁻¹]	V_{total} [cm³ g⁻¹]	Pore size (nm)	Light resource[a]	Reaction time [h]	Yield[b] [%]	Reused times	Ref.
CF-HCP		2.25	+1.38/−0.87	1200	0.92	—	LED	6	>99	5	217
BBT@TiO₂		2.11	—	129	0.11	—	LED	20	>99	—	218
CMP-BDD		2.06	+1.35/−0.71	605	0.59	2.9	LED	24	>99	5	221
PCP-MF		2.42	+1.67/−0.75	130	0.291	—	LED	20	96	5	222
EY-POP-1		—	—	587	0.33	—	LED	20	99	12	223
PhIm-2F-Ru		—	—	49	0.11	8.50	LED	72	98.5	4	214

Table 3 (*Contd.*)

CMPs	Chemical structure	Band gap [eV]	HOMO/LUMO [eV]/[eV]	S_{BET} [m² g⁻¹]	V_{total} [cm³ g⁻¹]	Pore size (nm)	Light resource[a]	Reaction time [h]	Yield[b] [%]	Reused times	Ref.
DA-CMP3		1.99	+1.14/−0.85	758	0.60	2.0–3.1	LED	1	99	10	225
P-Az-B		2.32	+1.14/−1.10	292	0.28	1.5	LED	24	93	5	224

[a] Ordinary household lamp. [b] Highest yield. RT: room temperature.

light irradiation.[232] These findings indicate that these CMP networks are excellent photocatalytic properties for organic conversion.

As an excellent platform, CMP materials not only have their own photocatalytic activity but also provide stable support for various photocatalytic materials for organic photocatalysis. The interface between CMPs and Pd NPs with heterojunction effects is beneficial for enhancing photocatalytic activity to the Suzuki coupling reaction.[233] The experimental results show that Pd@CMP has a right level of energy, uniformly dispersed Pd NPs (Fig. 17a), unique optical properties (Fig. 17b and c), and excellent photocatalytic performances (yield: 98%, under visible light). The electrons generated by the semiconductive polymer B-BO$_3$ are transferred to the active center of Pd NPs and attack the C–I bond of iodobenzene in the reaction, which promotes the completion of the reaction under visible light irradiation (Fig. 17e). Meanwhile, Pd@B-BO$_3$ is easily separated from the reaction substrate and recycled, which does not cause a big loss of activity in further reactions. The same strategy also can be applied to other classic C–C coupling reactions such as Heck reactions, Sonogashira reactions, and so on.

Few studies have so far used direct natural light as a source of photocatalytic technology. Light sources have always been the main part of the long-term cost of photocatalytic technology. To reduce the cost of photocatalytic organic conversion, it is necessary to explore the photocatalytic organic conversion of direct natural light. The CMP-CSU6 derived from 1,3,5-tri(9*H*-carbazol-9-yl)benzene synthesized by using the FeCl$_3$-mediated Friedel–Crafts reaction showed a high BET surface area (1022 m² g⁻¹) and adjustable band gap range.[234] It can effectively photocatalyze the conversion of hydrazine at room temperature under natural light and can retain its original photocatalytic activity after at least five cycles. Furthermore, a metal-free truxene-based CMP (Tx-CMP) has a narrow band gap (2.6 eV) with the ability to catalyze the oxidation of amines under direct sunlight.[235] Tx-CMPs with a high BET surface area and flake structures are synthesized by introducing a Tx molecule into CMPs. Their appropriate band gap is favorable for promoting photocatalytic oxidation reactions. Compared with TiO$_2$ and SG-CN, Tx-CMP photocatalysts have higher catalytic activity (conversion > 99%) for catalyzing the oxidative isotype coupling reaction of amines owing to their high BET surface area and suitable band gap. It should be noted that the high catalytic activity and selectivity of Tx-CMPs driven by sunlight can be maintained for at least five cycles. The carriers, holes, and electrons generated after Tx-CMPs absorb light are used to drive the reaction (Fig. 18). The latest research is still going on, expecting photocatalytic technology to bring more "light" to our lives.

6. CMPs for photocatalytic degradation of organic dyes

With the progress of industrialization, the discharge of a large number of organic pollutants into the environment poses a great threat to the ecological environment.[236–240] Among them,

6456 | *J. Mater. Chem. A*, 2020, **8**, 6434–6470

This journal is © The Royal Society of Chemistry 2020

Fig. 17 (a) TEM image of B-BO$_3$ immobilized with Pd NPs with sizes between 5 and 10 nm. (b) UV/vis DR spectra of Pd@B-BO$_3$ and B-BO$_3$. (c) VB and CB band positions of Pd@B-BO$_3$ and B-BO$_3$ (*vs.* SCE) determined by cyclic voltammetry. (d) Polymer backbone structure of B-BO$_3$. (e) Suggested reaction mechanism of photocatalytic Suzuki coupling *via* the light-induced heterojunction at the interface of B-BO$_3$ and Pd NPs. Reprinted with permission from ref. 233. Copyright 2015 American Chemical Society.

organic dyes are some of the most common contaminants, and they are widely concerned because they are non-biodegradable and carcinogenic. In order to ensure the safety of the ecological environment, it is urgent to develop an efficient, low-energy and sustainable technology to remove organic dyes from water. For this purpose, emerging materials are used in the study of photocatalytic degradation of organic dyes.[241–244] Among them, CMPs are some of the most promising photocatalytic materials. These CMP materials combining high porosity with good solution dispersion can facilitate the uniform contact of heterogeneous materials with contaminants to increases the

photocatalytic degradation activity. Meanwhile, they can combine different electron donor and electron acceptor groups, changing the structure (such as nanospheres, nanorods, and nanofilms) to facilitate charge transfer and increase redox sites to enhance degradation efficiency. They are ideal photocatalysts with high activity, high stability, and recyclability for photocatalytic degradation of organic dyes (Table 4).[245–254]

The main active substances that promote degradation are singlet oxygen ($^1O_2$), superoxide radical ($^*O^{2-}$), photogenerated holes (h$^+$) and HO$^•$ that are produced in photocatalytic reactions. According to preliminary work prediction, the

Fig. 18 Synthesis and structure of Tx-CMP and proposed mechanism for the natural sunlight driven oxidative homocoupling of benzylamine. Reprinted with permission from ref. 235. Copyright 2018 American Chemical Society.

Table 4 Summary of the photocatalytic performances of CMPs for the degradation of organic dyes in water[a]

CMPs	Chemical structure	Band gap [eV]	HOMO/LUMO [eV]/[eV]	S_{BET} [m² g⁻¹]	V_{total} [cm³ g⁻¹]	Reaction conditions	Active species	Dye: degradation [%]	Reused times	Ref.
P-FL-BT-3		2.07	−5.10/−3.03	—	—	P-FL-BT-3 in water under 1 h of white light irradiation	$O_2^{\bullet-}$	Rh B: >90	10	245
PCP2		2.4	−6.0/−3.6	—	—	PCP2 in water under 200 min of white light irradiation with O_2	h^+	MB: ~80	—	246
UPC-CMP-1		1.76	—	416.4	0.174	UPC-CMP-1 DMF dispersion under 120 s of visible light irradiation with 10×10^{-3} M $NaHCO_3$	$O_2^{\bullet-}$	CR: 88.3	5	247
Bn-Anderson-CMP		—	—	218	—	Bn-Anderson-CMP in water under 40 min of visible light ($\lambda > 450$ nm) irradiation	$^1O_2$, H_2O_2	MB: ~100; RhB: >90	5	248
Py-BF-CMP		1.55	−5.26/−3.71	1306	1.28	Py-BF-CMP in water under 1 h of visible light ($\lambda > 450$ nm) irradiation	$O_2^{\bullet-}$	RhB: 92	10	249
PDEB-1		1.95	+0.88/−1.07	1204	2.58	PDEB-1 in water under 1 h of visible light irradiation	$O_2^{\bullet-}$	RhB: 98	4	250
Py-POP		1.45	—	971	—	Py-POP in water under 80 min of visible light irradiation	$^1O_2$, $^{\bullet}OH$	RhB: ~100	—	251
Fc-TEB-CMP		2.98	+1.13/−1.85	984	1.29	Fc-TEB-CMP in water under 2 h of visible light irradiation	h^+, $^1O_2$, $^{\bullet}OH$	MB: ~98	5	252
CMPGA2		—	—	—	—	CMPGA2 in water under 80 min of the light reaction	h^+	MO: 89.2	3–5	253

6458 | *J. Mater. Chem. A*, 2020, **8**, 6434–6470

This journal is © The Royal Society of Chemistry 2020

Table 4 (*Contd.*)

CMPs	Chemical structure	Band gap [eV]	HOMO/LUMO [eV]/[eV]	S_{BET} [m² g⁻¹]	V_{total} [cm³ g⁻¹]	Reaction conditions	Active species	Dye: degradation [%]	Reused times	Ref.
TiO₂@PPS		2.36	—	—	—	TiO₂@PPs in water under 90 min of visible light	h⁺, ·OH	RhB: >99; MB: >98; MO: >93	—	254

This journal is © The Royal Society of Chemistry 2020

J. Mater. Chem. A, 2020, **8**, 6434–6470 | **6459**

mechanism of the photocatalytic degradation pathway of rhodamine B (RhB) by using metallophthalocyanine-based CMPs (MPC-CMPs) is as follows:[255–258]

$$MPc\text{-}CMP \xrightarrow{h\nu} {}^{1}MPc^*\text{-}CMP \xrightarrow{ISC} {}^{3}MPc^*\text{-}CMP \quad (1)$$

$$^{3}MPc^*\text{-}CMP + O_2 \rightarrow MPc^{\bullet+}\text{-}CMP + O_2^{\bullet-} \quad (2)$$

$$^{3}MPc^*\text{-}CMP + RhB \rightarrow MPc^{\bullet-}\text{-}CMP + RhB^{\bullet+} \quad (3)$$

$$MPc^{\bullet-}\text{-}CMP + O_2 \rightarrow MPc\text{-}CMP + O_2^{\bullet-} \quad (4)$$

$$O_2^{\bullet-} + H^+ \rightarrow HO_2^{\bullet} \quad (5)$$

$$HO_2^{\bullet} + H_2O \rightarrow H_2O_2 + OH^{\bullet} \quad (6)$$

$$H_2O_2 + h\nu \rightarrow 2\, OH^{\bullet} \quad (7)$$

$$HO_2^{\bullet} + RhB\text{-}H \rightarrow H_2O_2 + RhB^{\bullet} \quad (8)$$

$$RhB, RhB^{\bullet+}, RhB^{\bullet} + radicals \rightarrow CO_2, H_2O \quad (9)$$
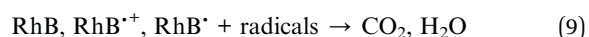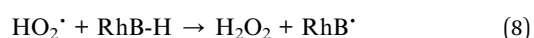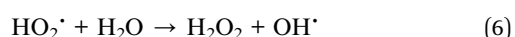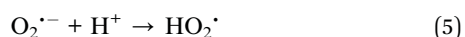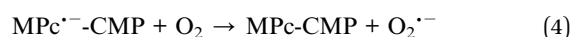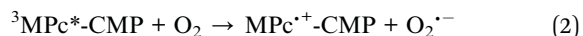
(ISC: intersystem crossing).

In the above formula, MPc-CMP is converted to an intermediate singlet state by photoexcitation, and then converted to a triplet state by an ISC transition [eqn (1)]. $^{3}MPc^*$-CMP reacts with molecular oxygen to convert to a free radical cation form of MPc-CMP and $O_2^{\bullet-}$ [eqn (2)]. Meanwhile, $^{3}MPc^*$-CMP oxidizes RhB to a free radical cationic form and produces a free radical anionic form of MPc-CMP [eqn (3)]. The free radical anion of MPc-CMP reacts with oxygen [eqn (4)], and $O_2^{\bullet-}$ is protonated to produce $HO_2^{\bullet}$ [eqn (5)]. Meanwhile, $OH^{\bullet}$ radicals are formed [eqn (6)], and they can also be generated when hydrogen peroxide is excited by light [eqn (7)]. These free radicals from the above reactions are the main active substances to degrade organic dyes [eqn (8) and (9)].

Highly dispersed nanostructured CMPs (CMP NPs) exhibit high photocatalytic activity for the degradation of organic dyes under the illumination of household lamps.[259] Various monomers used for different CMP NPs as well as their design principle and the synthesis route are shown in Fig. 19a. Scanning electron microscope (SEM) and transmission electron microscope (TEM) images of CMP NPs are shown in Fig. 19b. The morphology of synthetic CMPs is related to their monomers such as those containing triple bonds, which have a more rigid and expanded network backbone than CMPs containing single bonds. These CMPs are excited by light to generate photogenerated electron–hole pairs, and then they are separated and migrate to the valence band (VB) and conduction band (CB)
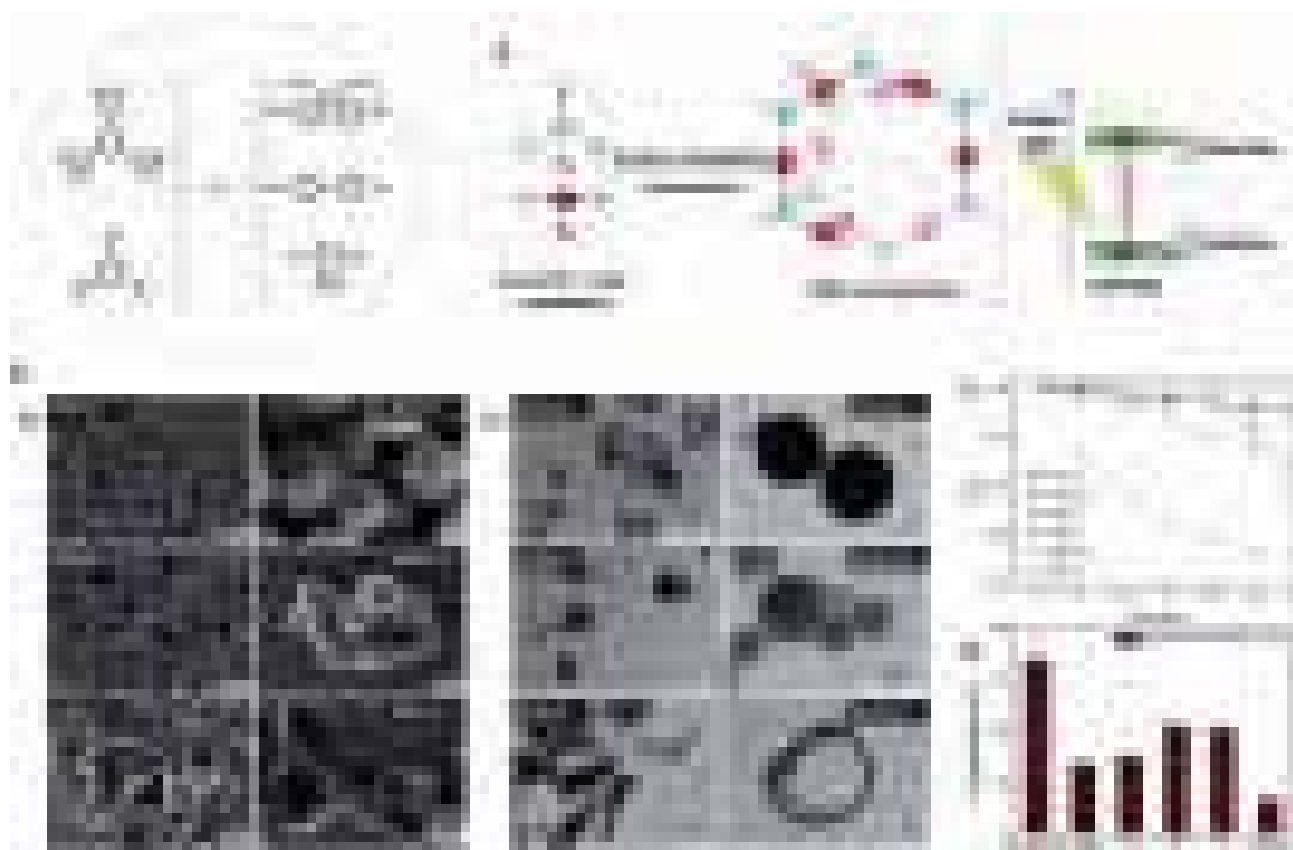
Fig. 19 (a) Various monomers used for different CMP NPs and their design principle and synthesis; (b) SEM (b₁) and TEM (b₂) images of CMP NPs with different shapes; (c) photocatalytic degradation of RhB in the presence of CMP NPs in water; (d) the effect of different scavengers, sodium azide (NaN₃), ammonium oxalate (AO), benzoquinone (BQ), isopropanol (IP) and the absence of oxygen (under N₂) on the degradation of RhB over B-BT₃-b under 30 min of visible light irradiation. Reprinted with permission from ref. 259. Copyright the Royal Society of Chemistry 2015.

6460 | J. Mater. Chem. A, 2020, 8, 6434–6470

This journal is © The Royal Society of Chemistry 2020

as redox sites for redox reactions. The results show that they can efficiently degrade RhB in water (degradation: 80%, 25 min) because the high dispersion of CMP NPs leads to many surface-active sites (Fig. 19c). $^1O_2$ is the main active substance for photocatalytic degradation of RhB proved by Fig. 19d. Meanwhile, these photocatalysts can be recycled many times without inactivation, which provides an economically viable solution for photocatalytic degradation of organic dyes.

Using the same composition strategy, new Anderson-type polyoxometalate (POM) built-in CMPs constructed from two tetrabromo-bifunctionalized Anderson-type POMs $(TBA)_3$ $\{MnMo_6O_{18}[(OCH_2)_3CNH(C_7H_3Br_2O)]_2\}$ (1) and $(TBA)_3\{MnMo_6$-$O_{18}[(OCH_2)_3CNH(C_5HBr_2OS)]_2\}$ (2) are obtained for the first time (Fig. 20a).[260] SEM and TEM images demonstrate the morphology of these two CMP NPs (Fig. 20b). These two POM-based CMP NPs have a diameter of about 30 nm and with a homogeneous distribution. They show a broad absorption band for efficient photocatalytic degradation of organic dyes. RhB degradation and methylene blue (MB) degradation both are >99% in the presence of these CMP photocatalysts under 1 h of visible light source irradiation at room temperature (Fig. 20c and b), and $^1O_2$ and H_2O_2 are the main active substances for the degradation of organic dyes. Then recycling experiments proved these photocatalysts can be cycled in the photocatalytic degradation of MB at least five times without reduction in catalytic activity (Fig. 20e). Improving the stability and increasing the

number of reusable times of photocatalysis are beneficial to reduce the cost of photocatalysis technologies.

The stability and recoverability of photocatalysts are critical to their availability in various photocatalytic applications including photocatalytic degradation of organic dyes. However, a common problem is that the catalytic activity of organic dyes makes them easily dissolved and dissociated in the reaction medium and prone to photobleaching, which hinders the recovery and long-term use of photocatalysts. Nanostructures have a high surface-to-volume ratio and porous materials have a larger surface area, which is conducive to solving this problem. With a high surface-to-volume ratio and large surface area, CMPs are a powerful platform for the design of stable and easily recycled new metal-free heterogeneous photocatalysts. As two quintessential examples, the degradation rate of organic dyes degraded by P-FL-BT-3 (ref. 245) or Py-BF-CMP[249] in water under 1 h of visible light irradiation is higher than 90% and they can be reused 10 times without inactivation (Table 4).

Recently, novel phthalocyanine-based CMPs (α-ZnPc-CMP and β-ZnPc-CMP) with a rigid linker are copolymerized by using zinc phthalocyanine (ZnPc) and 4,6-diaminoresorcinol dihydrochloride (DADHC) for promoting the cycle times of photocatalysts in the degradation of organic dyes.[261] These CMPs have a highly ordered skeleton arrangement and a two-dimensional (2D) open channel structure, which is advantageous for solving the problem of ZnPc aggregation to avoid
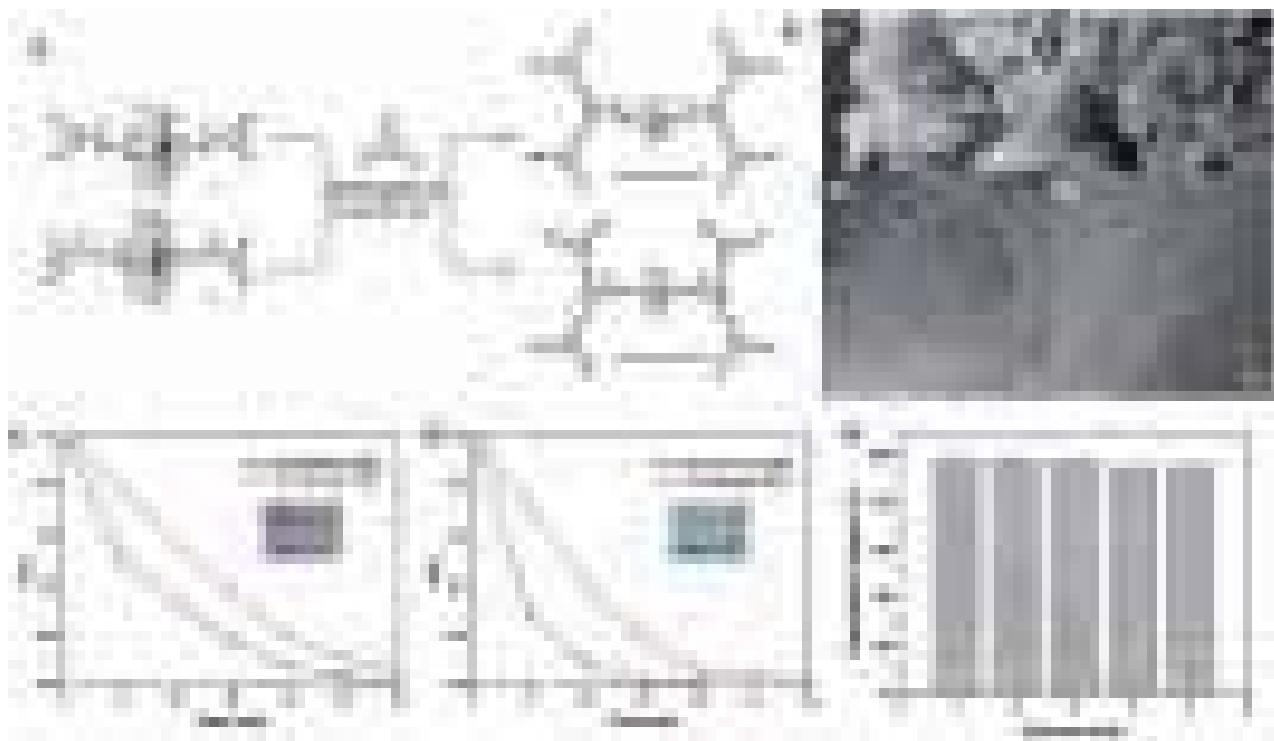
Fig. 20 (a) Synthesis routes of the two POM cluster-based CMPs; (b) SEM images of CMPs. (b₁) Bn-Anderson-CMP and (b₂) Th-AndersonCMP (the scale bars are 500 nm) and high-resolution TEM images of the POM cluster-based CMP samples re-dispersed in MeOH, revealing the inherent porous structures of (b₃) Bn-Anderson-CMP and (b₄) Th-Anderson-CMP (the scale bars are 5 nm). Photocatalytic degradation of dyes RhB (c) and MB (d) in the presence of POM cluster-based CMPs in water. (e) Recycling experiments of Bn-Anderson-CMP for the photocatalytic degradation of MB. Reprinted with permission from ref. 260. Copyright the Royal Society of Chemistry 2017.

This journal is © The Royal Society of Chemistry 2020

J. Mater. Chem. A, 2020, 8, 6434–6470 | 6461

secondary pollution and improve the recyclability of the photocatalysts. Insoluble α-ZnPc-CMP and β-ZnPc-CMP are treated with different solvents such as water, various organic solvents, strong hydrochloric acid and a high concentration of sodium hydroxide for 24 h to test the stability of these CMP photocatalysts. The results prove that they are stable in different solvents and can be reused for photocatalytic reactions after simple filtration.

CMPs and their composite materials provide a path worthy of further exploration for application in removing organic dyes from water. A series of metal phthalocyanine-based CMP (MPC-CMP) materials[258] and benzobisoxazole-linked porphyrin-based CMPs (BBO-Por-CMPs and BBO-MPor-CMPs)[262] were first synthesized for photocatalytic degradation of high concentrations of organic dyes, which have a fully conjugated system and are a class of non-toxic, stable photocatalysts. The specific surface area and backbone structure of CMPs are key factors affecting photocatalytic activity for the degradation of organic dyes because a higher specific surface area can increase the amount of adsorption of contaminants. Meanwhile, the linear polymer exhibits a narrower bandgap and higher charge transfer efficiency because they have a better extended conjugated system.[263] Furthermore, composite photocatalysts composed of TiO_2 and CMPs have enhanced photocatalytic ability to degrade organic dyes.[264] The photocatalytic degradation rate of the TrCMP-TiO_2 composite prepared by the hydrothermal method is several times higher than that of the TiO_2 material alone and other similar photocatalysts,[265,266] which can remove 96% MB under 1 h of visible light irradiation.

7. CMPs for photocatalytic sterilization and disinfection

Photocatalytic technologies are being actively researched in the fields of environment and medicine.[267–269] A large number of pollutants produced by human activities and harmful bacteria occurring in nature pose a great threat to human health and the ecological environment.[270] Especially the emergence of resistant bacteria is one of the main challenges facing modern public health.[271–274] As an antibacterial material, CMPs can produce large amounts of singlet oxygen ($^1O_2$) under visible light illumination in antibacterial photodynamic therapy,[81,92,259,275] which can inactivate bacteria (Fig. 21).[226,276,277] These materials have two forms: (i) evenly dispersed in water, which can inactivate bacteria in water under visible light, and (ii) hydrogel nanofiber membranes, which inhibit bacterial growth under visible light conditions and to provide continuous protection for the wound.

High-efficiency photosensitive CMP NPs synthesized by combining an electron-withdrawing group to a network structure with electron supply properties by using the Suzuki–Miyaura reaction are used as a class of highly effective photosensitizing antibacterial agents (Fig. 22a).[278] They are highly dispersed in aqueous solution and produce $^1O_2$ under visible light irradiation to effectively kill bacteria in water (Fig. 22b). Furthermore, a hydantoin group is introduced into a CMP

Fig. 21 Schematic illustration of the antibacterial mechanism of light active CMPs for sterilization and disinfection. A large amounts of $^1O_2$ is produced by photoactive CMPs which inactivates bacteria present in the surrounding environment.

network (CMPH) to prepare a novel CMP antibacterial agent.[279] The antibacterial agent can be fabricated not only into a single piece of nanoporous foam but also on other inert materials to produce a low-cost bactericidal material for medical supplies. In a simple one-pot reaction vessel, CMPH alters the permeability of the bacterial cell membrane, which causes bacteria (such as *E. coli*, *Staphylococcus aureus*, *etc.*) inactivation. These findings open a versatile door to the design and manufacture of CMP antimicrobial materials. A wide variety of photosensitive antibacterial agents can be produced by introducing different antibacterial substituents into CMP networks. Interestingly, a new type of hydrogel nanofiber membrane has recently emerged which exhibits visible-light-driven disinfection. The CMP NPs are embedded in polyethylene hydrogel nanofibers by a colloid-electrospinning process and crosslinked into nanofiber films under glutaraldehyde/HCl vapor conditions.[280] This synthetic strategy allows for flexible combination of different CMP NPs with different nanofiber support materials. These nanofiber films exhibit high biocompatibility and they will be
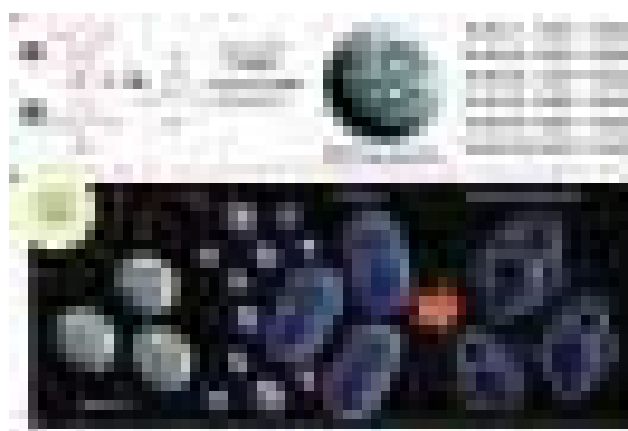

Fig. 22 (a) The structures and synthetic route of CMP NPs; (b) representative illustration of the mechanism for the inactivation of bacteria using CMP NPs. Reprinted with permission from ref. 278. Copyright the Royal Society of Chemistry 2016.

6462 | *J. Mater. Chem. A*, 2020, **8**, 6434–6470

This journal is © The Royal Society of Chemistry 2020

a promising candidate for a new generation of wound dressings given their photoactivity.

8. Conclusions and prospects

In recent years, CMPs have been extensively studied and developed for photocatalysis. This review mentions CMPs as a promising platform for photocatalytic applications covering water splitting, CO_2 reduction, organic conversion, and degradation of organic dyes, as well as sterilization and disinfection. Although these materials have proven to be excellent promising photocatalysts, more efforts are still needed to compete with more traditional and mature photocatalysts, which needs to be paid great attention in the following aspects in the future.

8.1 Design and synthesis

Most of the synthetic methods of CMP photocatalysts involve noble metal-catalyzed C–C cross-coupling reactions. Industrial and commercial applications of CMPs have been limited because they have some disadvantages such as high cost, harsh reaction conditions, and limited metal reserves. Meanwhile, trace metals remaining on the surface of CMPs are difficult to remove by purification. The effect of residual trace metals on the photocatalytic performances of CMPs needs to be clarified.

A wide variety of synthetic conditions are available to polymerize various functional group monomers but it is also promising to find suitable synthetic strategies for introducing photocatalytically active components into CMP networks for more challenging reactions. There are many CMP materials in this category, but not every CMP material has photocatalytic activity. Encapsulation of a metal dipyridine complex or a noble metal nanoparticle with a plasma effect in a CMP channel is an attractive strategy for the preparation of robust composite photocatalytic materials.

However, this method is also accompanied by some problems such as the encapsulated functional components easily leach from the porous framework, resulting in catalyst deactivation and environmental pollution. Solving this problem will help to improve the catalytic activity and service life of composite photocatalysts and improve their economic viability and bring about a wider range of industrial and commercial applications. Furthermore, it is necessary to find inexpensive and scalable synthetic methods to form CMPs. We developed CMPs for photocatalysis with the aim of finding cleaner production methods. Therefore, it is necessary to pay attention to the principle of sustainable development while improving the properties of the materials.

8.2 Morphology, molecular structure, and porosity

CMPs are rigid and distorted organic molecules linked by covalent bonds. Strong covalent bond connections impede the formation of reversible bonds, which creates an inherent disadvantage of CMP materials that they are completely amorphous. The amorphous powder morphology of CMPs is detrimental to their photocatalytic applications. In recent years, the morphology of CMPs has oriented towards diversity for further development, such as the advancement of other morphologies (e.g. nanofilm, nanoparticle, nanorod, and nanotube). They will provide more possibilities for applications of CMPs. Meanwhile, in order to design better CMP photocatalysts, more efforts are needed in the following directions: (i) further studies of exciton migration and charge carrier migration of CMPs are needed, which improves the charge transfer and conductivity of these polymers, thereby improving their photocatalytic performances; (ii) the molecular structure and photocatalytic performances of CMP materials need to be clarified systematically; (iii) further research on synthesizing low bandgap CMPs is required.

Space-efficient packing of polymer chains is effectively barred within these structures forming a large free volume, such structures being referred to as microporous structures. CMPs provide a powerful means of controlling microporous structures, pore environment and function. The surface area of these microporous materials usually exceeds 1000 m^2 g^{-1}. However, the BET surface area and pore volume of CMPs still need to be improved to enhance photocatalytic performances. The mainly research directions are as follows: (i) improvement of polymerization and crosslinking of CMPs, which can help to increase the BET surface area of these materials; (ii) reduction of the flexibility of the monomer link, which can reduce the length of the pillars between the monomer molecules, which requires the use of short, rigid comonomers; (iii) dimension control of CMPs, which helps to increase the BET surface area, for example, 3D structures of CMPs generally have a higher surface area than 2D CMPs.

8.3 Solar conversion efficiency

In order to popularize photocatalysis technology, improve the utilization efficiency of solar energy and reduce the cost are the main measures. The energy consumption of artificial light sources is one of the main factors responsible for the high cost of photocatalysis. Therefore, it is of long-term significance to explore the photocatalytic process of using natural sunlight. In order to efficiently use direct sunlight to reduce the cost of photocatalysis, the research has two trends: (i) one is building an efficient light-harvesting system at the molecular level to efficiently absorb solar energy that radiates onto the surfaces of CMPs; (ii) the other is designing a good external light absorption system, also known as an optical trap, to allow more sunlight irradiation on the surface of CMPs.

8.4 Catalytic stability

Stability is an important and universal challenge facing polymer porous materials. Synthetic polymer-based porous materials require mechanical stability, and most applications of porous solids require stability at least in air. These new materials have sufficient thermal stability in the process of heterogeneous catalysis at lower temperatures. For other applications, such as carbon dioxide capture, these materials are required to be stable under wet, acidic conditions.[281] As photocatalysts, these materials are required to maintain long-term stability under intense light irradiation.[140] CMPs are generally chemically stable; however, we

This journal is © The Royal Society of Chemistry 2020

J. Mater. Chem. A, 2020, **8**, 6434–6470 | **6463**

believe that further studies should be performed on their stability before they can be used commercially. For example, the long-term photochemical stability of CMPs deserves to be discussed in more detail. Especially in synthetic organic conversion, the use of long-term stable CMPs as heterogeneous photocatalysts helps to reduce the use of expensive metals and simplify the recovery and reuse of catalysts.

8.5 Application prospects

In general, these polymer-based porous materials are synthesized from monomers with hydrophobic groups and/or bio-repulsive groups. Hydrophilicity and biocompatibility issues need to be considered when attempting to compare these materials with enzyme systems and other commercial catalysts in applications including biosensors, electrocatalytic water splitting, and energy storage. The simple use of monomers with hydrophilic and/or biocompatible groups in the synthesis process of polymers could destroy the overall binding of the polymers and affect their photoelectric properties. Post-synthetic modification[282,283] is expected to be a solution to this problem. Furthermore, in the field of photoelectric catalysis, the energy level matching of the highest occupied molecular orbital (HOMOs) and lowest unoccupied molecular orbitals (LUMOs) between the components of the device facilitates the maximum energy conversion efficiency. Designing a reliable and clear method or technique to help adjust the HOMO and LUMO levels of CMPs could lead to a major advance in these materials.

CMPs are not crystalline, so they have more flexibility in design than crystalline COFs, and are more likely to be applied in the design of multi-component, multi-functional catalysts. In order for these materials to have greater industrial application, it is necessary to optimize multiple properties, such as the pore structure, surface area, stability, adsorption kinetics, and workability. As an excellent material platform, CMPs have thousands of monomers, and a single solution cannot solve all the problems. Therefore, it can be challenging to choose the right monomer for a particular application. Theoretical calculations and artificial intelligence (AI) could provide additional insights for determining the best material structure for specific applications.

As CMPs have many inherent advantages such as monomer diversity, adjustable molecular structures and morphologies, and stable conductive properties, there is potential in developing these polymers for photocatalytic applications. Combining the state-of-the-art advances of materials science, theoretical calculations and artificial intelligence, CMP materials and photocatalytic technology will be able to achieve more development and innovation. We hope this review can provide a useful guide for future developments in materials science and photocatalytic technology to solve challenging environmental and energy issues.

Author contributions

S. H. L., Z. T. Z., G. M. Z., Z. F. L., and R. X. conceived the study, analyzed the cited references and wrote the paper. All authors discussed the details of the article and commented on the manuscript.

Conflicts of interest

There are no conflicts of interest to declare.

Acknowledgements

Notes and references

1 J. I. Lewis, D. G. Fridley, L. K. Price, H. Lu and J. P. Romankiewicz, *Science*, 2015, **350**, 1034–1036.

2 D. Shindell and C. J. Smith, *Nature*, 2019, **573**, 408–411.

3 D. Tong, Q. Zhang, Y. Zheng, K. Caldeira, C. Shearer, C. Hong, Y. Qin and S. J. Davis, *Nature*, 2019, **572**, 373–377.

4 Y. Wang, H. Suzuki, J. Xie, O. Tomita, D. J. Martin, M. Higashi, D. Kong, R. Abe and J. Tang, *Chem. Rev.*, 2018, **118**, 5201–5241.

5 J. J. Zhang, H. Wang, X. Z. Yuan, G. M. Zeng, W. G. Tu and S. B. Wang, *J. Photochem. Photobiol., C*, 2019, **38**, 1–26.

6 J. Gong, C. Li and M. R. Wasielewski, *Chem. Soc. Rev.*, 2019, **48**, 1862–1864.

7 D. Gust and T. A. Moore, *Science*, 1989, **244**, 35–41.

8 F. Wen and C. Li, *Acc. Chem. Res.*, 2013, **46**, 2355–2364.

9 M. D. Kärkäs, O. Verho, E. V. Johnston and B. Åkermark, *Chem. Rev.*, 2014, **114**, 11863–12001.

10 M.-Q. Yang, N. Zhang, M. Pagliaro and Y.-J. Xu, *Chem. Soc. Rev.*, 2014, **43**, 8240–8254.

11 L. Sun, *Science*, 2015, **348**, 635.

12 M. Rudolf, S. V. Kirner and D. M. Guldi, *Chem. Soc. Rev.*, 2016, **45**, 612–630.

13 B. Zhang and L. Sun, *Chem. Soc. Rev.*, 2019, **48**, 2216–2264.

14 A. Fujishima and K. Honda, *Nature*, 1972, **238**, 37–38.

15 A. Fujishima, X. T. Zhang and D. A. Tryk, *Surf. Sci. Rep.*, 2008, **63**, 515–582.

16 T. P. Yoon, M. A. Ischay and J. Du, *Nat. Chem.*, 2010, **2**, 527–532.

17 W. Zhen, J. Ma and G. Lu, *Appl. Catal., B*, 2016, **190**, 12–25.

18 X. Hao, Z. Jin, H. Yang, G. Lu and Y. Bi, *Appl. Catal., B*, 2017, **210**, 45–56.

19 H. Wang, X. Liu, S. Wang and L. Li, *Appl. Catal., B*, 2018, **222**, 209–218.

20 D. Huang, S. Chen, G. Zeng, X. Gong, C. Zhou, M. Cheng, W. Xue, X. Yan and J. Li, *Coord. Chem. Rev.*, 2019, **385**, 44–80.

6464 | *J. Mater. Chem. A*, 2020, **8**, 6434–6470

This journal is © The Royal Society of Chemistry 2020

21 S. Chen, D. Huang, G. Zeng, X. Gong, W. Xue, J. Li, Y. Yang, C. Zhou, Z. Li, X. Yan, T. Li and Q. Zhang, *Chem. Eng. J.*, 2019, **370**, 1087–1100.

22 S. Luo, Z. Zeng, G. Zeng, Z. Liu, R. Xiao, M. Chen, L. Tang, W. Tang, C. Lai, M. Cheng, B. Shao, Q. Liang, H. Wang and D. Jiang, *ACS Appl. Mater. Interfaces*, 2019, **11**, 32579–32598.

23 M. Neumann, S. Fuldner, B. Konig and K. Zeitler, *Angew. Chem., Int. Ed.*, 2011, **50**, 951–954.

24 M. L. Marin, L. Santos-Juanes, A. Arques, A. M. Amat and M. A. Miranda, *Chem. Rev.*, 2012, **112**, 1710–1750.

25 X. Huang, X. Qi, F. Boey and H. Zhang, *Chem. Soc. Rev.*, 2012, **41**, 666–686.

26 R. Lin, L. Shen, Z. Ren, W. Wu, Y. Tan, H. Fu, J. Zhang and L. Wu, *Chem. Commun.*, 2014, **50**, 8533–8535.

27 F. Chen, Q. Yang, Y. Zhong, H. An, J. Zhao, T. Xie, Q. Xu, X. Li, D. Wang and G. Zeng, *Water Res.*, 2016, **101**, 555–563.

28 L. Zhang, C. G. Niu, C. Liang, X. J. Wen, D. W. Huang, H. Guo, X. F. Zhao and G. M. Zeng, *Chem. Eng. J.*, 2018, **352**, 863–875.

29 S. Cao, J. Low, J. Yu and M. Jaroniec, *Adv. Mater.*, 2015, **27**, 2150–2176.

30 Y. Yang, C. Zhang, D. L. Huang, G. M. Zeng, J. H. Huang, C. Lai, C. Y. Zhou, W. J. Wang, H. Guo, W. J. Xue, R. Deng, M. Cheng and W. P. Xiong, *Appl. Catal., B*, 2019, **245**, 87–99.

31 D. L. Huang, Z. H. Li, G. M. Zeng, C. Y. Zhou, W. J. Xue, X. M. Gong, X. L. Yan, S. Chen, W. J. Wang and M. Cheng, *Appl. Catal., B*, 2019, **240**, 153–173.

32 J. Huang, J. Hu, Y. Shi, G. Zeng, W. Cheng, H. Yu, Y. Gu, L. Shi and K. Yi, *J. Colloid Interface Sci.*, 2019, **541**, 356–366.

33 L. Jiang, X. Yuan, G. Zeng, J. Liang, Z. Wu, H. Yu, D. Mo, H. Wang, Z. Xiao and C. Zhou, *J. Colloid Interface Sci.*, 2019, **536**, 17–29.

34 Z. M. Zhang, T. Zhang, C. Wang, Z. Lin, L. S. Long and W. Lin, *J. Am. Chem. Soc.*, 2015, **137**, 3197–3200.

35 X.-J. Kong, Z. Lin, Z.-M. Zhang, T. Zhang and W. Lin, *Angew. Chem., Int. Ed.*, 2016, **55**, 6411–6416.

36 J. J. Walsh, A. M. Bond, R. J. Forster and T. E. Keyes, *Coord. Chem. Rev.*, 2016, **306**, 217–234.

37 D. Huang, X. Yan, M. Yan, G. Zeng, C. Zhou, J. Wan, M. Cheng and W. Xue, *ACS Appl. Mater. Interfaces*, 2018, **10**, 21035–21055.

38 W. Xue, D. Huang, J. Li, G. Zeng, R. Deng, Y. Yang, S. Chen, Z. Li, X. Gong and B. Li, *Chem. Eng. J.*, 2019, **373**, 1144–1157.

39 D. Huang, Z. Li, G. Zeng, C. Zhou, W. Xue, X. Gong, X. Yan, S. Chen, W. Wang and M. Cheng, *Appl. Catal., B*, 2019, **240**, 153–173.

40 Y. Liu, M. Cheng, Z. Liu, G. Zeng, H. Zhong, M. Chen, C. Zhou, W. Xiong, B. Shao and B. Song, *Chemosphere*, 2019, **236**, 124387.

41 T. Xu, X. Liu, S. Wang and L. Li, *Nano-Micro Lett.*, 2019, **11**, 37.

42 P. Sudarsanam, E. Peeters, E. V. Makshina, V. I. Parvulescu and B. F. Sels, *Chem. Soc. Rev.*, 2019, **48**, 2366–2421.

43 R. J. White, R. Luque, V. L. Budarin, J. H. Clark and D. J. Macquarrie, *Chem. Soc. Rev.*, 2009, **38**, 481–494.

44 B. H. Wu and N. F. Zheng, *Nano Today*, 2013, **8**, 168–197.

45 L. Chen, Y. Honsho, S. Seki and D. L. Jiang, *J. Am. Chem. Soc.*, 2010, **132**, 6742–6748.

46 H. Wang, Z. Zeng, P. Xu, L. Li, G. Zeng, R. Xiao, Z. Tang, D. Huang, L. Tang, C. Lai, D. Jiang, Y. Liu, H. Yi, L. Qin, S. Ye, X. Ren and W. Tang, *Chem. Soc. Rev.*, 2019, **48**, 488–516.

47 T. Xu, S. Wang, L. Li and X. Liu, *Appl. Catal., A*, 2019, **575**, 132–141.

48 S. Linic, P. Christopher and D. B. Ingram, *Nat. Mater.*, 2011, **10**, 911–921.

49 C.-C. Wang, J.-R. Li, X.-L. Lv, Y.-Q. Zhang and G. Guo, *Energy Environ. Sci.*, 2014, **7**, 2831–2867.

50 T. Zhang and W. Lin, *Chem. Soc. Rev.*, 2014, **43**, 5982–5993.

51 T. Banerjee, K. Gottschling, G. Savasci, C. Ochsenfeld and B. V. Lotsch, *ACS Energy Lett.*, 2018, **3**, 400–409.

52 J. X. Jiang, F. Su, A. Trewin, C. D. Wood, N. L. Campbell, H. Niu, C. Dickinson, A. Y. Ganin, M. J. Rosseinsky, Y. Z. Khimyak and A. I. Cooper, *Angew. Chem., Int. Ed.*, 2007, **46**, 8574–8578.

53 Y. Xu, S. Jin, H. Xu, A. Nagai and D. Jiang, *Chem. Soc. Rev.*, 2013, **42**, 8012–8031.

54 G. Zhang, Z.-A. Lan and X. Wang, *Angew. Chem., Int. Ed.*, 2016, **55**, 15712–15727.

55 K. Zhang, Z. Vobecka, K. Tauer, M. Antonietti and F. Vilela, *Chem. Commun.*, 2013, **49**, 11158–11160.

56 J. X. Jiang, Y. Y. Li, X. F. Wu, J. L. Xiao, D. J. Adams and A. I. Cooper, *Macromolecules*, 2013, **46**, 8779–8783.

57 Z. J. Wang, S. Ghasimi, K. Landfester and K. A. Zhang, *Chem. Commun.*, 2014, **50**, 8177–8180.

58 Z. J. Wang, S. Ghasimi, K. Landfester and K. A. I. Zhang, *J. Mater. Chem. A*, 2014, **2**, 18720–18724.

59 M. Sener, J. Strumpfer, J. Hsin, D. Chandler, S. Scheuring, C. N. Hunter and K. Schulten, *Chemphyschem*, 2011, **12**, 518–531.

60 M. K. Sener, J. D. Olsen, C. N. Hunter and K. Schulten, *Proc. Natl. Acad. Sci. U. S. A.*, 2007, **104**, 15723–15728.

61 M. Sener, J. Strumpfer, J. A. Timney, A. Freiberg, C. N. Hunter and K. Schulten, *Biophys. J.*, 2010, **99**, 67–75.

62 R. P. Goncalves, J. Busselez, D. Levy, J. Seguin and S. Scheuring, *J. Struct. Biol.*, 2005, **149**, 79–86.

63 C. Uragami, Y. Sugai, K. Hanjo, A. Sumino, R. Fujii, T. Nishioka, I. Kinoshita, T. Dewa, M. Nango, A. T. Gardiner, R. J. Cogdell and H. Hashimoto, *J. Photochem. Photobiol., A*, 2015, **313**, 60–71.

64 D. Murat, M. Byrne and A. Komeili, *Cold Spring Harbor Perspect. Biol.*, 2010, **2**, a000422.

65 J. Hsin, J. Strumpfer, M. Sener, P. Qian, C. N. Hunter and K. Schulten, *New J. Phys.*, 2010, **12**, 085005.

66 L. Chen, Y. Honsho, S. Seki and D. Jiang, *J. Am. Chem. Soc.*, 2010, **132**, 6742–6748.

67 K. V. Rao, R. Haldar, T. K. Maji and S. J. George, *Phys. Chem. Chem. Phys.*, 2016, **18**, 156–163.

68 B. G. Kim, X. Ma, C. Chen, Y. Ie, E. W. Coir, H. Hashemi, Y. Aso, P. F. Green, J. Kieffer and J. Kim, *Adv. Funct. Mater.*, 2013, **23**, 439–445.

69 B. Keller, A. McLean, B. G. Kim, K. Chung, J. Kim and T. Goodson, *J. Phys. Chem. C*, 2016, **120**, 9088–9096.

This journal is © The Royal Society of Chemistry 2020

J. Mater. Chem. A, 2020, **8**, 6434–6470 | **6465**

70 A. Casey, S. D. Dimitrov, P. Shakya-Tuladhar, Z. P. Fei, M. Nguyen, Y. Han, T. D. Anthopoulos, J. R. Durrant and M. Heeney, *Chem. Mater.*, 2016, **28**, 5110–5120.

71 Y. Y. Yu, T. W. Tsai and C. P. Chen, *J. Phys. Chem. C*, 2018, **122**, 24585–24591.

72 R. H. Friend, R. W. Gymer, A. B. Holmes, J. H. Burroughes, R. N. Marks, C. Taliani, D. D. C. Bradley, D. A. D. Santos, J. L. Brédas, M. Lögdlund and W. R. Salaneck, *Nature*, 1999, **397**, 121–128.

73 A. J. Berresheim, M. Muller and K. Mullen, *Chem. Rev.*, 1999, **99**, 1747–1786.

74 U. H. Bunz, *Chem. Rev.*, 2000, **100**, 1605–1644.

75 U. Scherf and E. J. W. List, *Adv. Mater.*, 2002, **14**, 477–487.

76 J. X. Jiang, F. Su, H. Niu, C. D. Wood, N. L. Campbell, Y. Z. Khimyak and A. I. Cooper, *Chem. Commun.*, 2008, 486–488, DOI: 10.1039/b715563h.

77 J. X. Jiang, F. Su, A. Trewin, C. D. Wood, H. Niu, J. T. Jones, Y. Z. Khimyak and A. I. Cooper, *J. Am. Chem. Soc.*, 2008, **130**, 7710–7720.

78 J. Weber and A. Thomas, *J. Am. Chem. Soc.*, 2008, **130**, 6334–6335.

79 A. I. Cooper, *Adv. Mater.*, 2009, **21**, 1291–1295.

80 J. Schmidt, M. Werner and A. Thomas, *Macromolecules*, 2009, **42**, 4426–4429.

81 Z. J. Wang, S. Ghasimi, K. Landfester and K. A. Zhang, *Adv. Mater.*, 2015, **27**, 6265–6270.

82 J. Schmidt, J. Weber, J. D. Epping, M. Antonietti and A. Thomas, *Adv. Mater.*, 2009, **21**, 702–705.

83 Y. Xu, L. Chen, Z. Guo, A. Nagai and D. Jiang, *J. Am. Chem. Soc.*, 2011, **133**, 17622–17625.

84 G. Cheng, T. Hasell, A. Trewin, D. J. Adams and A. I. Cooper, *Angew. Chem., Int. Ed.*, 2012, **51**, 12727–12731.

85 Y. Xu, A. Nagai and D. Jiang, *Chem. Commun.*, 2013, **49**, 1591–1593.

86 C. Gu, N. Huang, J. Gao, F. Xu, Y. Xu and D. Jiang, *Angew. Chem., Int. Ed.*, 2014, **53**, 4850–4855.

87 B. Bonillo, R. S. Sprick and A. I. Cooper, *Chem. Mater.*, 2016, **28**, 3469–3480.

88 X. Li, Z. Li and Y. W. Yang, *Adv. Mater.*, 2018, **30**, 1800177.

89 Y. Xu, N. Mao, S. Feng, C. Zhang, F. Wang, Y. Chen, J. Zeng and J.-X. Jiang, *Macromol. Chem. Phys.*, 2017, **218**, 1700049.

90 Y. Xu, C. Zhang, P. Mu, N. Mao, X. Wang, Q. He, F. Wang and J.-X. Jiang, *Sci. China: Chem.*, 2017, **60**, 1075–1083.

91 C. Yang, B. C. Ma, L. Zhang, S. Lin, S. Ghasimi, K. Landfester, K. A. Zhang and X. Wang, *Angew. Chem., Int. Ed.*, 2016, **55**, 9202–9206.

92 K. Zhang, D. Kopetzki, P. H. Seeberger, M. Antonietti and F. Vilela, *Angew. Chem., Int. Ed.*, 2013, **52**, 1432–1436.

93 M. G. Schwab, M. Hamburger, X. Feng, J. Shu, H. W. Spiess, X. Wang, M. Antonietti and K. Mullen, *Chem. Commun.*, 2010, **46**, 8932–8934.

94 J. X. Jiang, A. Trewin, D. J. Adams and A. I. Cooper, *Chem. Sci.*, 2011, **2**, 1777–1781.

95 L. Li, Z. Cai, Q. Wu, W. Y. Lo, N. Zhang, L. X. Chen and L. Yu, *J. Am. Chem. Soc.*, 2016, **138**, 7681–7686.

96 Y. Xu, N. Mao, C. Zhang, X. Wang, J. Zeng, Y. Chen, F. Wang and J.-X. Jiang, *Appl. Catal., B*, 2018, **228**, 1–9.

97 L. Li, W.-y. Lo, Z. Cai, N. Zhang and L. Yu, *Macromolecules*, 2016, **49**, 6903–6909.

98 K. Kailasam, M. B. Mesch, L. Mohlmann, M. Baar, S. Blechert, M. Schwarze, M. Schroder, R. Schomacker, J. Senker and A. Thomas, *Energy Technol.*, 2016, **4**, 744–750.

99 R. S. Sprick, J. X. Jiang, B. Bonillo, S. Ren, T. Ratvijitvech, P. Guiglion, M. A. Zwijnenburg, D. J. Adams and A. I. Cooper, *J. Am. Chem. Soc.*, 2015, **137**, 3265–3270.

100 P. B. Pati, G. Damas, L. Tian, D. L. A. Fernandes, L. Zhang, I. B. Pehlivan, T. Edvinsson, C. M. Araujo and H. N. Tian, *Energy Environ. Sci.*, 2017, **10**, 1372–1376.

101 C. Gu, Y. Chen, Z. Zhang, S. Xue, S. Sun, K. Zhang, C. Zhong, H. Zhang, Y. Pan, Y. Lv, Y. Yang, F. Li, S. Zhang, F. Huang and Y. Ma, *Adv. Mater.*, 2013, **25**, 3443–3448.

102 C. Gu, N. Huang, Y. Chen, L. Qin, H. Xu, S. Zhang, F. Li, Y. Ma and D. Jiang, *Angew. Chem., Int. Ed.*, 2015, **54**, 13594–13598.

103 F. Wei, X. Cai, J. Nie, F. Wang, C. Lu, G. Yang, Z. Chen, C. Ma and Y. Zhang, *Polym. Chem.*, 2018, **9**, 3832–3839.

104 Y. Liu, Z. Liao, X. Ma and Z. Xiang, *ACS Appl. Mater. Interfaces*, 2018, **10**, 30698–30705.

105 W.-Y. Huang, Z.-Q. Shen, J.-Z. Cheng, L.-L. Liu, K. Yang, X. Chen, H.-R. Wen and S.-Y. Liu, *J. Mater. Chem. A*, 2019, **7**, 24222–24230.

106 H.-J. Hou, X.-H. Zhang, D.-K. Huang, X. Ding, S.-Y. Wang, X.-L. Yang, S.-Q. Li, Y.-G. Xiang and H. Chen, *Appl. Catal., B*, 2017, **203**, 563–571.

107 J. Chen, X. Tao, L. Tao, H. Li, C. Li, X. Wang, C. Li, R. Li and Q. Yang, *Appl. Catal., B*, 2019, **241**, 461–470.

108 K. Maeda, *ACS Catal.*, 2013, **3**, 1486–1503.

109 T. Hisatomi, J. Kubota and K. Domen, *Chem. Soc. Rev.*, 2014, **43**, 7520–7535.

110 J. Ran, J. Zhang, J. Yu, M. Jaroniec and S. Z. Qiao, *Chem. Soc. Rev.*, 2014, **43**, 7787–7812.

111 Y. F. Zhao, B. Li, Q. Wang, W. Gao, C. L. J. Wang, M. Wei, D. G. Evans, X. Duan and D. O'Hare, *Chem. Sci.*, 2014, **5**, 951–958.

112 S. J. A. Moniz, S. A. Shevlin, D. J. Martin, Z.-X. Guo and J. Tang, *Energy Environ. Sci.*, 2015, **8**, 731–759.

113 Y. F. Zhao, X. D. Jia, G. I. N. Waterhouse, L. Z. Wu, C. H. Tung, D. O'Hare and T. R. Zhang, *Adv. Energy Mater.*, 2016, **6**, 1501974.

114 M. Karayilan, W. P. Brezinski, K. E. Clary, D. L. Lichtenberger, R. S. Glass and J. Pyun, *Angew. Chem., Int. Ed.*, 2019, **131**, 7617–7630.

115 K. Mazloomi and C. Gomes, *Renewable Sustainable Energy Rev.*, 2012, **16**, 3024–3033.

116 J. Chen, X. P. Tao, L. Tao, H. Li, C. Z. Li, X. L. Wang, C. Li, R. G. Li and Q. H. Yang, *Appl. Catal., B*, 2019, **241**, 461–470.

117 Z. A. Lan, W. Ren, X. Chen, Y. F. Zhang and X. C. Wang, *Appl. Catal., B*, 2019, **245**, 596–603.

118 L. Schlapbach and A. Zuttel, *Nature*, 2001, **414**, 353–358.

119 N. S. Lewis and D. G. Nocera, *Proc. Natl. Acad. Sci. U. S. A.*, 2006, **103**, 15729–15735.

120 A. W. C. van den Berg and C. O. Areán, *Chem. Commun.*, 2008, 668–681, DOI: 10.1039/b712576n.

6466 | *J. Mater. Chem. A*, 2020, **8**, 6434–6470

This journal is © The Royal Society of Chemistry 2020

121 P. Jena, *J. Phys. Chem. Lett.*, 2011, **2**, 206–211.

122 G. Zhang, Z. A. Lan and X. Wang, *Angew. Chem., Int. Ed.*, 2016, **55**, 15712–15727.

123 H. Wang, B. Hou, Y. Yang, Q. Chen, M. Zhu, A. Thomas and Y. Liao, *Small*, 2018, **14**, 1803232.

124 V. S. Mothika, P. Sutar, P. Verma, S. Das, S. K. Pati and T. K. Maji, *Chemistry*, 2019, **25**, 3867–3874.

125 G. Q. Zhang, W. Ou, J. Wang, Y. S. Xu, D. Xu, T. Sun, S. N. Xiao, M. R. Wang, H. X. Li, W. Chen and C. L. Su, *Appl. Catal., B*, 2019, **245**, 114–121.

126 K. Ding, Q. Zhang, Q. Li and S. Ren, *Macromol. Chem. Phys.*, 2019, **220**, 1900304.

127 C. Cheng, X. Wang, Y. Lin, L. He, J.-X. Jiang, Y. Xu and F. Wang, *Polym. Chem.*, 2018, **9**, 4468–4475.

128 A. Bhunia, D. Esquivel, S. Dey, R. Fernandez-Teran, Y. Goto, S. Inagaki, P. Van der Voort and C. Janiak, *J. Mater. Chem. A*, 2016, **4**, 13450–13457.

129 G. Zhang, W. Ou, J. Wang, Y. Xu, D. Xu, T. Sun, S. Xiao, M. Wang, H. Li, W. Chen and C. Su, *Appl. Catal., B*, 2019, **245**, 114–121.

130 C. B. Meier, R. S. Sprick, A. Monti, P. Guiglion, J.-S. M. Lee, M. A. Zwijnenburg and A. I. Cooper, *Polymer*, 2017, **126**, 283–290.

131 C. Cheng, X. Wang and F. Wang, *Appl. Surf. Sci.*, 2019, **495**, 143537.

132 J. Yu, X. Sun, X. Xu, C. Zhang and X. He, *Appl. Catal., B*, 2019, **257**, 117935.

133 L. Guo, Y. Niu, S. Razzaque, B. Tan and S. Jin, *ACS Catal.*, 2019, **9**, 9438–9445.

134 K. Lin, Z. Wang, Z. Hu, P. Luo, X. Yang, X. Zhang, M. Rafiq, F. Huang and Y. Cao, *J. Mater. Chem. A*, 2019, **7**, 19087–19093.

135 R. S. Sprick, Y. Bai, A. A. Y. Guilbert, M. Zbiri, C. M. Aitchison, L. Wilbraham, Y. Yan, D. J. Woods, M. A. Zwijnenburg and A. I. Cooper, *Chem. Mater.*, 2019, **31**, 305–313.

136 L. Guo, Y. Niu, H. Xu, Q. Li, S. Razzaque, Q. Huang, S. Jin and B. Tan, *J. Mater. Chem. A*, 2018, **6**, 19775–19781.

137 S. Bi, Z.-A. Lan, S. Paasch, W. Zhang, Y. He, C. Zhang, F. Liu, D. Wu, X. Zhuang, E. Brunner, X. Wang and F. Zhang, *Adv. Funct. Mater.*, 2017, **27**, 1703146.

138 D. Schwarz, Y. S. Kochergin, A. Acharjya, A. Ichangi, M. V. Opanasenko, J. Cejka, U. Lappan, P. Arki, J. He, J. Schmidt, P. Nachtigall, A. Thomas, J. Tarabek and M. J. Bojdys, *Chem.–Eur. J.*, 2017, **23**, 13023–13027.

139 M. G. Schwab, M. Hamburger, X. Feng, J. Shu, H. W. Spiess, X. Wang, M. Antonietti and K. Müllen, *Chem. Commun.*, 2010, **46**, 8932–8934.

140 R. S. Sprick, J.-X. Jiang, B. Bonillo, S. Ren, T. Ratvijitvech, P. Guiglion, M. A. Zwijnenburg, D. J. Adams and A. I. Cooper, *J. Am. Chem. Soc.*, 2015, **137**, 3265–3270.

141 J. Cai, P. Ruffieux, R. Jaafar, M. Bieri, T. Braun, S. Blankenburg, M. Muoth, A. P. Seitsonen, M. Saleh, X. Feng, K. Müllen and R. Fasel, *Nature*, 2010, **466**, 470–473.

142 R. S. Sprick, B. Bonillo, M. Sachs, R. Clowes, J. R. Durrant, D. J. Adams and A. I. Cooper, *Chem. Commun.*, 2016, **52**, 10008–10011.

143 K. V. Rao, S. Mohapatra, C. Kulkarni, T. K. Maji and S. J. George, *J. Mater. Chem.*, 2011, **21**, 12958–12963.

144 A. Modak, K. Yamanaka, Y. Goto and S. Inagaki, *Bull. Chem. Soc. Jpn.*, 2016, **89**, 887–891.

145 A. Modak, Y. Maegawa, Y. Goto and S. Inagaki, *Polym. Chem.*, 2016, **7**, 1290–1296.

146 Y. F. Xu, C. Zhang, P. Mu, N. Mao, X. Wang, Q. He, F. Wang and J. X. Jiang, *Sci. China: Chem.*, 2017, **60**, 1075–1083.

147 Y. F. Xu, N. Mao, S. Feng, C. Zhang, F. Wang, Y. Chen, J. H. Zeng and J. X. Jiang, *Macromol. Chem. Phys.*, 2017, **218**, 1700049.

148 Z. J. Wang, X. Y. Yang, T. J. Yang, Y. B. Zhao, F. Wang, Y. Chen, J. H. Zeng, C. Yan, F. Huang and J. X. Jiang, *ACS Catal.*, 2018, **8**, 8590–8596.

149 Y. Bai, L. Wilbraham, B. J. Slater, M. A. Zwijnenburg, R. S. Sprick and A. I. Cooper, *J. Am. Chem. Soc.*, 2019, **141**, 9063–9071.

150 K. L. Materna, R. H. Crabtree and G. W. Brudvig, *Chem. Soc. Rev.*, 2017, **46**, 6099–6110.

151 D. Kong, Y. Zheng, M. Kobielusz, Y. Wang, Z. Bai, W. Macyk, X. Wang and J. Tang, *Mater. Today*, 2018, **21**, 897–924.

152 R. Eisenberg and H. B. Gray, *Inorg. Chem.*, 2008, **47**, 1697–1699.

153 L. Duan, F. Bozoglian, S. Mandal, B. Stewart, T. Privalov, A. Llobet and L. Sun, *Nat. Chem.*, 2012, **4**, 418–423.

154 S. Jayanthi, D. V. S. Muthu, N. Jayaraman, S. Sampath and A. K. Sood, *Chemistryselect*, 2017, **2**, 4522–4532.

155 L. Wang, Y. Wan, Y. Ding, Y. Niu, Y. Xiong, X. Wu and H. Xu, *Nanoscale*, 2017, **9**, 4090–4096.

156 Z. Wang, C. Li and K. Domen, *Chem. Soc. Rev.*, 2019, **48**, 2109–2125.

157 S. Chen, T. Takata and K. Domen, *Nat. Rev. Mater.*, 2017, **2**, 17050.

158 L. Wang, Y. Zhang, L. Chen, H. Xu and Y. Xiong, *Adv. Mater.*, 2018, **30**, 1801955.

159 G. Zhang, Z.-A. Lan and X. Wang, *Chem. Sci.*, 2017, **8**, 5261–5274.

160 H. Yu, R. Shi, Y. Zhao, G. I. N. Waterhouse, L.-Z. Wu, C.-H. Tung and T. Zhang, *Adv. Mater.*, 2016, **28**, 9454–9477.

161 M. G. Walter, E. L. Warren, J. R. McKone, S. W. Boettcher, Q. Mi, E. A. Santori and N. S. Lewis, *Chem. Rev.*, 2011, **111**, 5815.

162 K. Maeda and K. Domen, *J. Phys. Chem. Lett.*, 2010, **1**, 2655–2661.

163 L. Liao, Q. Zhang, Z. Su, Z. Zhao, Y. Wang, Y. Li, X. Lu, D. Wei, G. Feng, Q. Yu, X. Cai, J. Zhao, Z. Ren, H. Fang, F. Robles-Hernandez, S. Baldelli and J. Bao, *Nat. Nanotechnol.*, 2014, **9**, 69–73.

164 J. Liu, Y. Liu, N. Liu, Y. Han, X. Zhang, H. Huang, Y. Lifshitz, S.-T. Lee, J. Zhong and Z. Kang, *Science*, 2015, **347**, 970.

165 K. Maeda, T. Takata, M. Hara, N. Saito, Y. Inoue, H. Kobayashi and K. Domen, *J. Am. Chem. Soc.*, 2005, **127**, 8286–8287.

166 V. S. Vyas, V. W.-h. Lau and B. V. Lotsch, *Chem. Mater.*, 2016, **28**, 5191–5204.

This journal is © The Royal Society of Chemistry 2020

J. Mater. Chem. A, 2020, **8**, 6434–6470 | **6467**

167 V. S. Vyas, F. Haase, L. Stegbauer, G. Savasci, F. Podjaski, C. Ochsenfeld and B. V. Lotsch, *Nat. Commun.*, 2015, **6**, 8508.

168 L. Li, Z. Cai, Q. Wu, W.-Y. Lo, N. Zhang, L. X. Chen and L. Yu, *J. Am. Chem. Soc.*, 2016, **138**, 7681–7686.

169 V. S. Vyas and B. V. Lotsch, *Nature*, 2015, **521**, 41–42.

170 R. S. Sprick, B. Bonillo, R. Clowes, P. Guiglion, N. J. Brownbill, B. J. Slater, F. Blanc, M. A. Zwijnenburg, D. J. Adams and A. I. Cooper, *Angew. Chem., Int. Ed.*, 2016, **55**, 1792–1796.

171 X. Wang, K. Maeda, A. Thomas, K. Takanabe, G. Xin, J. M. Carlsson, K. Domen and M. Antonietti, *Nat. Mater.*, 2009, **8**, 76–80.

172 J. Wirth, R. Neumann, M. Antonietti and P. Saalfrank, *Phys. Chem. Chem. Phys.*, 2014, **16**, 15917–15926.

173 D. J. Martin, P. J. T. Reardon, S. J. A. Moniz and J. Tang, *J. Am. Chem. Soc.*, 2014, **136**, 12568–12571.

174 S. Yang, Y. Gong, J. Zhang, L. Zhan, L. Ma, Z. Fang, R. Vajtai, X. Wang and P. M. Ajayan, *Adv. Mater.*, 2013, **25**, 2452–2456.

175 K. Schwinghammer, M. B. Mesch, V. Duppel, C. Ziegler, J. Senker and B. V. Lotsch, *J. Am. Chem. Soc.*, 2014, **136**, 1730–1733.

176 L. Wang, Y. Wan, Y. Ding, S. Wu, Y. Zhang, X. Zhang, G. Zhang, Y. Xiong, X. Wu, J. Yang and H. Xu, *Adv. Mater.*, 2017, **29**, 1702428.

177 J. Zhou, X. Gao, R. Liu, Z. Xie, J. Yang, S. Zhang, G. Zhang, H. Liu, Y. Li, J. Zhang and Z. Liu, *J. Am. Chem. Soc.*, 2015, **137**, 7596–7599.

178 G. Zhang, Z.-A. Lan, L. Lin, S. Lin and X. Wang, *Chem. Sci.*, 2016, **7**, 3062–3066.

179 K. C. Nicolaou, Y. H. Lim and J. Becker, *Angew. Chem., Int. Ed.*, 2009, **48**, 3444–3448.

180 Y. Liu, Y. Yang, Q. Sun, Z. Wang, B. Huang, Y. Dai, X. Qin and X. Zhang, *ACS Appl. Mater. Interfaces*, 2013, **5**, 7654–7658.

181 A. Listorti, J. Durrant and J. Barber, *Nat. Mater.*, 2009, **8**, 929–930.

182 O. K. Varghese, M. Paulose, T. J. Latempa and C. A. Grimes, *Nano Lett.*, 2009, **9**, 731–737.

183 Y. Izumi, *Coord. Chem. Rev.*, 2013, **257**, 171–186.

184 W. Tu, Y. Zhou and Z. Zou, *Adv. Mater.*, 2014, **26**, 4607–4626.

185 S. Bandyopadhyay, A. G. Anil, A. James and A. Patra, *ACS Appl. Mater. Interfaces*, 2016, **8**, 27669–27678.

186 I. Omae, *Catal. Today*, 2006, **115**, 33–52.

187 M. Vogt, M. Gargir, M. A. Iron, Y. Diskin-Posner, Y. Ben-David and D. Milstein, *Chemistry*, 2012, **18**, 9194–9197.

188 C. A. Huff, J. W. Kampf and M. S. Sanford, *Organometallics*, 2012, **31**, 4643–4645.

189 F. M. Wisser, P. Berruyer, L. Cardenas, Y. Mohr, E. A. Quadrelli, A. Lesage, D. Farrusseng and J. Canivet, *ACS Catal.*, 2018, **8**, 1653–1661.

190 C. Yang, W. Huang, L. C. da Silva, K. A. I. Zhang and X. Wang, *Chemistry*, 2018, **24**, 17454–17458.

191 X. Yu, Z. Yang, B. Qiu, S. Guo, P. Yang, B. Yu, H. Zhang, Y. Zhao, X. Yang, B. Han and Z. Liu, *Angew. Chem., Int. Ed.*, 2019, **58**, 632–636.

192 H. Zhong, Z. Hong, C. Yang, L. Li, Y. Xu, X. Wang and R. Wang, *Chemsuschem*, 2019, **12**, 4529–4537.

193 V. A. Montes, C. Pérez-Bolívar, N. Agarwal, J. Shinar and P. Anzenbacher, *J. Am. Chem. Soc.*, 2006, **128**, 12436–12438.

194 X. Huang, C. Zhu, S. Zhang, W. Li, Y. Guo, X. Zhan, Y. Liu and Z. Bo, *Macromolecules*, 2008, **41**, 6895–6902.

195 R. Ambre, K.-B. Chen, C.-F. Yao, L. Luo, E. W.-G. Diau and C.-H. Hung, *J. Phys. Chem. C*, 2012, **116**, 11907–11916.

196 J. Grodkowski, D. Behar, P. Neta and P. Hambright, *J. Phys. Chem. A*, 1997, **101**, 248–254.

197 D. Behar, T. Dhanasekaran, P. Neta, C. M. Hosten, D. Ejeh, P. Hambright and E. Fujita, *J. Phys. Chem. A*, 1998, **102**, 2870–2877.

198 K. Leung, I. M. B. Nielsen, N. Sai, C. Medforth and J. A. Shelnutt, *J. Phys. Chem. A*, 2010, **114**, 10174–10184.

199 I. Hod, M. D. Sampson, P. Deria, C. P. Kubiak, O. K. Farha and J. T. Hupp, *ACS Catal.*, 2015, **5**, 6302–6309.

200 X. Zhan, Z. a. Tan, B. Domercq, Z. An, X. Zhang, S. Barlow, Y. Li, D. Zhu, B. Kippelen and S. R. Marder, *J. Am. Chem. Soc.*, 2007, **129**, 7246–7247.

201 K. Kunal, C. G. Robertson, S. Pawlus, S. F. Hahn and A. P. Sokolov, *Macromolecules*, 2008, **41**, 7232–7238.

202 C. Cui, W.-Y. Wong and Y. Li, *Energy Environ. Sci.*, 2014, **7**, 2276–2284.

203 C. Chen, C. Tang, W. Xu, Y. Li and L. Xu, *Phys. Chem. Chem. Phys.*, 2018, **20**, 9536–9542.

204 L. Shi and W. Xia, *Chem. Soc. Rev.*, 2012, **41**, 7687–7697.

205 J. Xuan and W.-J. Xiao, *Angew. Chem., Int. Ed.*, 2012, **51**, 6828–6838.

206 M. Rueping, C. Vila, A. Szadkowska, R. M. Koenigs and J. Fronert, *ACS Catal.*, 2012, **2**, 2810–2815.

207 C. K. Prier, D. A. Rankic and D. W. C. MacMillan, *Chem. Rev.*, 2013, **113**, 5322–5363.

208 D. M. Schultz and T. P. Yoon, *Science*, 2014, **343**, 1239176.

209 L. Qin, H. Yi, G. Zeng, C. Lai, D. Huang, P. Xu, Y. Fu, J. He, B. Li and C. Zhang, *J. Hazard. Mater.*, 2019, **380**, 120864.

210 L. Qin, Z. Zeng, G. Zeng, C. Lai, A. Duan, R. Xiao, D. Huang, Y. Fu, H. Yi and B. Li, *Appl. Catal., B*, 2019, **259**, 118035.

211 Y. F. Zhi, K. Li, H. Xia, M. Xue, Y. Mu and X. M. Liu, *J. Mater. Chem. A*, 2017, **5**, 8697–8704.

212 C. Ayed, L. C. da Silva, D. Wang and K. A. I. Zhang, *J. Mater. Chem. A*, 2018, **6**, 22145–22151.

213 Y. F. Zhi, S. Ma, H. Xia, Y. M. Zhang, Z. Shi, Y. Mu and X. M. Liu, *Appl. Catal., B*, 2019, **244**, 36–44.

214 C. Monterde, R. Navarro, M. Iglesias and F. Sanchez, *ACS Appl. Mater. Interfaces*, 2019, **11**, 3459–3465.

215 W. Ou, G. Q. Zhang, J. Wu and C. L. Su, *ACS Catal.*, 2019, **9**, 5178–5183.

216 J. Luo, X. Zhang and J. Zhang, *ACS Catal.*, 2015, **5**, 2250–2254.

217 Y. Zhi, K. Li, H. Xia, M. Xue, Y. Mu and X. Liu, *J. Mater. Chem. A*, 2017, **5**, 8697–8704.

6468 | *J. Mater. Chem. A*, 2020, **8**, 6434–6470

This journal is © The Royal Society of Chemistry 2020

218 C. Ayed, W. Huang, R. Li, L. C. da Silva, D. Wang, O. Suraeva, W. Najjar and K. A. I. Zhang, *Part. Part. Syst. Charact.*, 2018, **35**, 1700234.

219 H. Bohra, P. Li, C. Yang, Y. Zhao and M. Wang, *Polym. Chem.*, 2018, **9**, 1972–1982.

220 W. Liu, S. Wu, Q. Su, B. Guo, P. Ju, G. Li and Q. Wu, *J. Mater. Sci.*, 2019, **54**, 1205–1212.

221 H. Zhang, Q. Huang, W. Zhang, C. Pan, J. Wang, C. Ai, J. Tang and G. Yu, *Chemphotochem*, 2019, **3**, 645–651.

222 Z. J. Wang, R. Li, K. Landfester and K. A. I. Zhang, *Polymer*, 2017, **126**, 291–295.

223 C.-A. Wang, Y.-W. Li, X.-L. Cheng, J.-P. Zhang and Y.-F. Han, *RSC Adv.*, 2017, **7**, 408–414.

224 S. Ghasimi, S. A. Bretschneider, W. Huang, K. Landfester and K. A. I. Zhang, *Adv. Sci.*, 2017, **4**, 1700101.

225 Y. Zhi, S. Ma, H. Xia, Y. Zhang, Z. Shi, Y. Mu and X. Liu, *Appl. Catal., B*, 2019, **244**, 36–44.

226 X. Ding and B. H. Han, *Angew. Chem., Int. Ed.*, 2015, **54**, 6536–6539.

227 N. Boens, V. Leen and W. Dehaen, *Chem. Soc. Rev.*, 2012, **41**, 1130–1172.

228 A. Kamkaew, S. H. Lim, H. B. Lee, L. V. Kiew, L. Y. Chung and K. Burgess, *Chem. Soc. Rev.*, 2013, **42**, 77–88.

229 H. Lu, J. Mack, Y. Yang and Z. Shen, *Chem. Soc. Rev.*, 2014, **43**, 4778–4823.

230 Y. Ni and J. Wu, *Org. Biomol. Chem.*, 2014, **12**, 3774–3791.

231 J. M. Tobin, J. Liu, H. Hayes, M. Demleitner, D. Ellis, V. Arrighi, Z. Xu and F. Vilela, *Polym. Chem.*, 2016, **7**, 6662–6670.

232 M. Liras, M. Iglesias and F. Sanchez, *Macromolecules*, 2016, **49**, 1666–1673.

233 Z. J. Wang, S. Ghasimi, K. Landfester and K. A. I. Zhang, *Chem. Mater.*, 2015, **27**, 1921–1924.

234 W. J. Zhang, J. T. Tang, W. G. Yu, Q. Huang, Y. Fu, G. C. Kuang, C. Y. Pan and G. P. Yu, *ACS Catal.*, 2018, **8**, 8084–8091.

235 V. R. Battula, H. Singh, S. Kumar, I. Bala, S. K. Pal and K. Kailasam, *ACS Catal.*, 2018, **8**, 6751–6759.

236 B. Song, G. Zeng, J. Gong, J. Liang, P. Xu, Z. Liu, Y. Zhang, C. Zhang, M. Cheng, Y. Liu, S. Ye, H. Yi and X. Ren, *Environ. Int.*, 2017, **105**, 43–55.

237 X. Y. Ren, G. M. Zeng, L. Tang, J. J. Wang, J. Wan, H. P. Feng, B. Song, C. Huang and X. Tang, *Soil Biol. Biochem.*, 2018, **116**, 70–81.

238 D. Hu, M. Shen, Y. Zhang and G. Zeng, *Sci. Total Environ.*, 2019, **657**, 108–110.

239 B. Shao, X. Liu, Z. Liu, G. Zeng, W. Zhang, Q. Liang, Y. Liu, Q. He, X. Yuan, D. Wang, S. Luo and S. Gong, *Chem. Eng. J.*, 2019, **374**, 479–493.

240 Y. Fu, P. Xu, D. Huang, G. Zeng, C. Lai, L. Qin, B. Li, J. He, H. Yi, M. Cheng and C. Zhang, *Appl. Surf. Sci.*, 2019, **473**, 578–588.

241 S. Tonda, S. Kumar, S. Kandula and V. Shanker, *J. Mater. Chem. A*, 2014, **2**, 6772–6780.

242 K. He, G. Q. Chen, G. M. Zeng, A. W. Chen, Z. Z. Huang, J. B. Shi, T. T. Huang, M. Peng and L. Hu, *Appl. Catal., B*, 2018, **228**, 19–28.

243 L. Tang, Y. I. Liu, J. J. Wang, G. M. Zeng, Y. C. Deng, H. R. Dong, H. P. Feng, J. J. Wang and B. Peng, *Appl. Catal., B*, 2018, **231**, 1–10.

244 D. N. Jiang, M. Chen, H. Wang, G. M. Zeng, D. L. Huang, M. Cheng, Y. Liu, W. J. Xue and Z. W. Wang, *Coord. Chem. Rev.*, 2019, **380**, 471–483.

245 S. Ghasimi, S. Prescher, Z. J. Wang, K. Landfester, J. Yuan and K. A. I. Zhang, *Angew. Chem., Int. Ed.*, 2015, **54**, 14549–14553.

246 L. Li and Z. Cai, *Polym. Chem.*, 2016, **7**, 4937–4943.

247 Z. Xiao, Y. Zhou, X. Xin, Q. Zhang, L. Zhang, R. Wang and D. Sun, *Macromol. Chem. Phys.*, 2016, **217**, 599–604.

248 Y. Li, M. Liu and L. Chen, *J. Mater. Chem. A*, 2017, **5**, 13757–13762.

249 B. Wang, Z. Xie, Y. Li, Z. Yang and L. Chen, *Macromolecules*, 2018, **51**, 3443–3449.

250 J. Wang, H. Yang, L. Jiang, S. Liu, Z. Hao, J. Cheng and G. Ouyang, *Catal. Sci. Technol.*, 2018, **8**, 5024–5033.

251 M. Li, H. Zhao and Z.-Y. Lu, *Microporous Mesoporous Mater.*, 2019, **292**, 109774.

252 L. Ma, Y. Liu, Y. Liu, S. Jiang, P. Li, Y. Hao, P. Shao, A. Yin, X. Feng and B. Wang, *Angew. Chem., Int. Ed.*, 2019, **58**, 4221–4226.

253 C. H. A. Tsang, J. Tobin, J. Xuan, F. Vilela, H. Huang and D. Y. C. Leung, *Appl. Catal., B*, 2019, **240**, 50–63.

254 C. Yang, N. Han, W. Zhang, W. Wang, W. Li, B. Xia, C. Han, Z. Cui and X. Zhang, *Chem. Eng. J.*, 2019, **374**, 1382–1393.

255 Y. Wang, A. D. Zhou, Y. Jiang, X. Y. Chen and J. B. He, *RSC Adv.*, 2015, **5**, 37823–37829.

256 Q. Liang, M. Zhang, C. H. Liu, S. Xu and Z. Y. Li, *Appl. Catal., A*, 2016, **519**, 107–115.

257 W. Lu, T. Xu, Y. Wang, H. Hu, N. Li, X. Jiang and W. Chen, *Appl. Catal., B*, 2016, **180**, 20–28.

258 Q. Li, H. G. Wang, Y. H. Li, Y. W. Li and Q. Duan, *Dyes Pigm.*, 2018, **149**, 261–267.

259 B. C. Ma, S. Ghasimi, K. Landfester, F. Vilela and K. A. I. Zhang, *J. Mater. Chem. A*, 2015, **3**, 16064–16071.

260 Y. S. Li, M. X. Liu and L. Chen, *J. Mater. Chem. A*, 2017, **5**, 13757–13762.

261 L. Cai, Y. Li, Y. Li, H. Wang, Y. Yu, Y. Liu and Q. Duan, *J. Hazard. Mater.*, 2018, **348**, 47–55.

262 Y. W. Li, Q. Duan, H. G. Wang, B. Gao, N. N. Qiu and Y. H. Li, *J. Photochem. Photobiol., A*, 2018, **356**, 370–378.

263 J. H. Wang, H. S. Yang, L. Jiang, S. Q. Liu, Z. P. Hao, J. Cheng and G. F. Ouyang, *Catal. Sci. Technol.*, 2018, **8**, 5024–5033.

264 J. S. Li, X. H. Wen, Q. J. Zhang and S. J. Ren, *RSC Adv.*, 2018, **8**, 34560–34565.

265 M. Bednarz, J. Lapin, R. McGillicuddy, K. M. Pelzer, G. S. Engel and G. B. Griffin, *J. Phys. Chem. C*, 2017, **121**, 5467–5479.

266 Y. G. Xiang, X. P. Wang, X. H. Zhang, H. J. Hou, K. Dai, Q. Y. Huang and H. Chen, *J. Mater. Chem. A*, 2018, **6**, 153–159.

267 X. Wang, Y. H. Liang, W. J. An, J. S. Hu, Y. F. Zhu and W. Q. Cui, *Appl. Catal., B*, 2017, **219**, 53–62.

This journal is © The Royal Society of Chemistry 2020

J. Mater. Chem. A, 2020, **8**, 6434–6470 | **6469**

268 Y. Guan, S. M. Wang, X. Wang, C. Sun, Y. Huang, C. Liu and H. Y. Zhao, *Appl. Catal., B*, 2017, **209**, 329–338.

269 Y. Liu, Z. Liu, D. Huang, M. Cheng, G. Zeng, C. Lai, C. Zhang, C. Zhou, W. Wang, D. Jiang, H. Wang and B. Shao, *Coord. Chem. Rev.*, 2019, **388**, 63–78.

270 R. P. Schwarzenbach, B. I. Escher, K. Fenner, T. B. Hofstetter, C. A. Johnson, U. von Gunten and B. Wehrli, *Science*, 2006, **313**, 1072–1077.

271 P. A. Smith and F. E. Romesberg, *Nat. Chem. Biol.*, 2007, **3**, 549–556.

272 R. Chait, A. Craney and R. Kishony, *Nature*, 2007, **446**, 668–671.

273 P. E. Sudbery, *Nat. Rev. Microbiol.*, 2011, **9**, 737–748.

274 Q. Zhang, G. Lambert, D. Liao, H. Kim, K. Robin, C. K. Tung, N. Pourmand and R. H. Austin, *Science*, 2011, **333**, 1764–1767.

275 H. Urakami, K. Zhang and F. Vilela, *Chem. Commun.*, 2013, **49**, 2353–2355.

276 A. P. Castano, P. Mroz and M. R. Hamblin, *Nat. Rev. Cancer*, 2006, **6**, 535–545.

277 M. Gruner, L. Tuchscherr, B. Loffler, D. Gonnissen, K. Riehemann, M. C. Staniford, U. Kynast and C. A. Strassert, *ACS Appl. Mater. Interfaces*, 2015, **7**, 20965–20971.

278 B. C. Ma, S. Ghasimi, K. Landfester and K. A. I. Zhang, *J. Mater. Chem. B*, 2016, **4**, 5112–5118.

279 F. Wang, F. Ren, D. Ma, P. Mu, H. J. Wei, C. H. Xiao, Z. Q. Zhu, H. X. Sun, W. D. Liang, J. X. Chen, L. H. Chen and A. Li, *J. Mater. Chem. A*, 2018, **6**, 266–274.

280 S. Jiang, B. C. Ma, W. Huang, A. Kaltbeitzel, G. Kizisavas, D. Crespy, K. A. I. Zhang and K. Landfester, *Nanoscale Horiz.*, 2018, **3**, 439–446.

281 R. T. Woodward, L. A. Stevens, R. Dawson, M. Vijayaraghavan, T. Hasell, I. P. Silverwood, A. V. Ewing, T. Ratvijitvech, J. D. Exley, S. Y. Chong, F. Blanc, D. J. Adams, S. G. Kazarian, C. E. Snape, T. C. Drage and A. I. Cooper, *J. Am. Chem. Soc.*, 2014, **136**, 9028–9035.

282 P. Lindemann, A. Schade, L. Monnereau, W. Feng, K. Batra, H. Gliemann, P. Levkin, S. Brase, C. Woll and M. Tsotsalas, *J. Mater. Chem. A*, 2016, **4**, 6815–6818.

283 B. Kiskan and J. Weber, *ACS Macro Lett.*, 2012, **1**, 37–40.